Kent Academic Repository

Reindl, Theresia, Giese, Sven, Greve, Johannes N., Reinke, Patrick Y., Chizhov, Igor, Latham, Sharissa L., Mulvihill, Daniel P., Taft, Manuel H. and Manstein, Dietmar J. (2022) *Distinct actin–tropomyosin cofilament populations drive the functional diversification of cytoskeletal myosin motor complexes.* iScience . ISSN 2589-0042.

Downloaded from

https://kar.kent.ac.uk/95379/ The University of Kent's Academic Repository KAR

The version of record is available from

https://doi.org/10.1016/j.isci.2022.104484

This document version

Author's Accepted Manuscript

DOI for this version

https://doi.org/10.1016/j.isci.2022.104484

Licence for this version

CC BY-NC-ND (Attribution-NonCommercial-NoDerivatives)

Additional information

Versions of research works

Versions of Record

If this version is the version of record, it is the same as the published version available on the publisher's web site. Cite as the published version.

Author Accepted Manuscripts

If this document is identified as the Author Accepted Manuscript it is the version after peer review but before type setting, copy editing or publisher branding. Cite as Surname, Initial. (Year) 'Title of article'. To be published in *Title of Journal* , Volume and issue numbers [peer-reviewed accepted version]. Available at: DOI or URL (Accessed: date).

Enquiries

If you have questions about this document contact ResearchSupport@kent.ac.uk. Please include the URL of the record in KAR. If you believe that your, or a third party's rights have been compromised through this document please see our Take Down policy (available from https://www.kent.ac.uk/guides/kar-the-kent-academic-repository#policies).

Journal Pre-proof

Distinct actin–tropomyosin cofilament populations drive the functional diversification of cytoskeletal myosin motor complexes

Theresia Reindl, Sven Giese, Johannes N. Greve, Patrick Y. Reinke, Igor Chizhov, Sharissa L. Latham, Daniel P. Mulvihill, Manuel H. Taft, Dietmar J. Manstein

Please cite this article as: Reindl, T., Giese, S., Greve, J.N., Reinke, P.Y., Chizhov, I., Latham, S.L., Mulvihill, D.P., Taft, M.H., Manstein, D.J., Distinct actin–tropomyosin cofilament populations drive the functional diversification of cytoskeletal myosin motor complexes, *ISCIENCE* (2022), doi: https://doi.org/10.1016/j.isci.2022.104484.

This is a PDF file of an article that has undergone enhancements after acceptance, such as the addition of a cover page and metadata, and formatting for readability, but it is not yet the definitive version of record. This version will undergo additional copyediting, typesetting and review before it is published in its final form, but we are providing this version to give early visibility of the article. Please note that, during the production process, errors may be discovered which could affect the content, and all legal disclaimers that apply to the journal pertain.
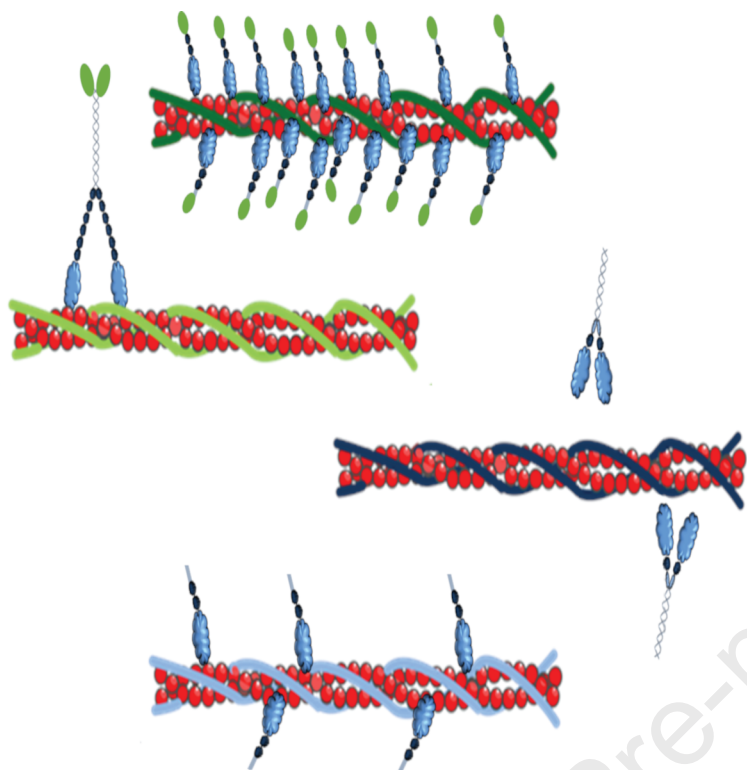
1 **Distinct actin–tropomyosin cofilament populations drive the functional diversification**

2 **of cytoskeletal myosin motor complexes**

3

4 Theresia Reindl[1, #a, †] and Sven Giese[1, †], Johannes N. Greve[1], Patrick Y. Reinke[1, #b], Igor

5 Chizhov[1], Sharissa L. Latham[1, #c], Daniel P. Mulvihill[2], Manuel H. Taft[1], and Dietmar J.

6 Manstein[1,3,4,§] *

7

8 From the [1] Institute for Biophysical Chemistry, Fritz–Hartmann–Centre for Medical

9 Research, Hannover Medical School, 30625 Hannover, Germany, [2] School of Biosciences,

10 University of Kent, Canterbury, Kent CT2 7NJ, UK, [3] Division for Structural Biochemistry,

11 Hannover Medical School, 30625 Hannover, Germany, [4] RESiST, Cluster of Excellence

12 2155, Medizinische Hochschule Hannover, 30625 Hannover, Germany

13

14 Current address: [#a] Department of Microbiology and Immunology, Stanford University School

15 of Medicine, 279 Campus Drive West, Stanford CA 94305, USA;; [#b] FS–BMX, Deutsches

16 Elektronen–Synchrotron DESY, Notkestraße 85, 22607 Hamburg, Germany; [#c] The Kinghorn

17 Cancer Centre, Garvan Institute of Medical Research, 370 Victoria St, Darlinghurst, Sydney,

18 NSW, 2010, Australia.

19

20 [†] These authors contributed equally to this work

21 * Corresponding author: Dietmar J. Manstein, Tel: (49) 511–5323700; Fax: (49) 511–

22 5325966; E–mail: manstein.dietmar@mh-hannover.de

23 [§] Lead contact

SUMMARY

The effects of N-terminal acetylation of the high molecular weight tropomyosin isoforms Tpm1.6 and Tpm2.1 and the low molecular weight isoforms Tpm1.12, Tpm3.1 and Tpm4.2 on the actin affinity and the thermal stability of actin-tropomyosin cofilaments are described. Furthermore, we show how the exchange of cytoskeletal tropomyosin isoforms and their N-terminal acetylation affects the kinetic and chemomechanical properties of cytoskeletal actin-tropomyosin-myosin complexes. Our results reveal the extent to which the different actin-tropomyosin-myosin complexes differ in their kinetic and functional properties. The maximum sliding velocity of the actin filament as well as the optimal motor density for continuous unidirectional movement, parameters that were previously considered to be unique and invariant properties of each myosin isoform, are shown to be influenced by the exchange of the tropomyosin isoform and the N-terminal acetylation of tropomyosin.

INTRODUCTION

Tropomyosins (Tpm) form a large family of polar, double stranded, α–helical coiled–coil actin filament binding proteins (McLachlan and Stewart, 1976; von der Ecken et al., 2015). The human Tpm genes are referred to as *TPM1* through *TPM4* (Geeves et al., 2015; Gunning et al., 2008; Lin et al., 1997). Variations in the DNA sequences of the coding regions of the four genes and alternative splicing of the variable exons, 1, 2, 6, and 9, gives rise to considerable molecular diversity (Figure 1A). As some Tpm splice isoforms are missing variable exon 2, this results in shorter and longer isoforms with 245 to 248 and 284 to 285 amino acid residues, respectively. Individual Tpm dimers interact with actin filaments only weakly, with dissociation constants estimated to be in the millimolar range (Tobacman, 2008; Wegner, 1980; Weigt et al., 1991). High–affinity binding occurs only upon polymerization into continuous Tpm cables on the actin filament surface (Fischer et al., 2016; Heald and Hitchcock-DeGregori, 1988; Vilfan, 2001; Wegner, 1980). This process is driven by the head–to–tail association of Tpm dimers (Fischer et al., 2016; Heald and Hitchcock-DeGregori, 1988; Vilfan, 2001; Wegner, 1980), and is further enhanced by the presence of myosin motors (Eaton, 1976; Moraczewska et al., 1999; Pathan-Chhatbar et al., 2018). In general, the dynamic nature of actin–Tpm (A–Tpm) interactions is characterized by high cooperativity and has been shown to influence the competitive association of actin binding proteins, such as fimbrin and cofilin (Christensen et al., 2017).

While some Tpm isoforms are specifically associated with muscle tissues, most isoforms function within the context of cytoskeletal A–Tpm cofilaments (Gunning et al., 2005; Pittenger

2

58 et al., 1994). Members of the Tpm family are thought to play a key role in coordinating the

59 interaction of cytoskeletal actin filaments with other types of actin–binding proteins by

60 defining the functional properties of individual actin filament populations. This idea took shape

61 in recent years after it was recognized that almost all actin filaments of the cytoskeleton exist

62 as cofilaments with Tpm isoforms (Meiring et al., 2018) and after various disease associations

63 became known (Marston et al., 2013; Redwood and Robinson, 2013; Reumiller et al., 2018).

64 Specifically, cytoskeletal Tpm isoforms have been linked to diseases affecting neurosensory

65 functions, platelet disorders and cancer (Brettle et al., 2016; Latham et al., 2018; Pleines et al.,

66 2017). Transformation and cancerous growth are frequently accompanied by upregulated

67 production of low molecular weight (LMW) Tpm isoforms, such as Tpm 3.1 and Tpm4.2, and

68 loss of high molecular weight (HMW) Tpm isoforms (Hendricks and Weintraub, 1981;

69 Kabbage et al., 2013; Stefen et al., 2018; Stehn et al., 2006). Thus, over–production of Tpm4.2

70 has been directly linked to the invasiveness of infiltrating breast cancer cells. In transformed

71 cells, Tpm3.1 accounts for up to 70% of total Tpm, as opposed to 25% in corresponding control

72 cells (Meiring et al., 2018). Compounds that manipulate actin function by directly targeting

73 Tpm3.1 are therefore attractive and promising anti–cancer agents (Bonello et al., 2016; Stehn

74 et al., 2013).

75 The regulation of myosin motor activity by A–Tpm cofilaments differs between sarcomeric

76 and cytoskeletal isoforms. In the context of muscle, calcium binding to troponin triggers a

77 series of conformational changes that shift the Tpm filament on F–actin to reveal the myosin–

78 binding interface on the actin filament (Parry and Squire, 1973; Spudich et al., 1972; Spudich

79 and Watt, 1971). In contrast to the muscle system, cytoskeletal actomyosin complexes function

80 in the absence of troponin or isofunctional troponin–like proteins and in the context of greater

81 Tpm isoform diversity. Cell–based and biochemical studies support the hypothesis that the

82 association of filamentous actin with different tropomyosin isoforms determines the identity

83 and modulates the activity of the interacting myosin motor proteins (Gateva et al., 2017;

84 Manstein and Mulvihill, 2016). Specifically, it has been shown that bipolar bundles of non–

85 muscle myosin–2 (NM–2) isoforms that function as integral components of stress fibres, actin

86 arcs and contractile rings, and the various unconventional myosin motors that support vesicle

87 and organelle transport, as well as discrete steps of endocytosis and exocytosis, are integrated

88 into the appropriate functional context by distinct A–Tpm cofilaments as schematically shown

89 in Figure 1B–E (Barua et al., 2018; Clayton et al., 2015; Kee et al., 2015; Meiring et al., 2019;

90 Sckolnick et al., 2016).

91   Corroborating evidence includes the observation that class 1 myosin–dependent delivery of

92   organelles to the perinuclear region is affected by the association of F–actin with Tpm1.7 but

93   not with Tpm3.1 (Pelham et al., 1996). Cargo structures that carry myosin–1C (Myo1C) on

94   their surface are regulated by Tpm1.6 with respect to their run initiation and run termination,

95   which may enable effective sorting of cargo by co–regulation of the initiation and termination

96   of kinesin–driven runs at actin/microtubule intersections (McIntosh et al., 2015). In the cortical

97   region of adipocytes, Tpm3.1 but not Tpm1.7 was proposed to define the actin population

98   regulating the recruitment of Myo1C and non–muscle myosin–2A (NM–2A), which are both

99   required for GLUT4–mediated glucose uptake and blood glucose clearance (Kee et al., 2015).

100   In stress fibers, the incorporation of the HMW splice isoforms Tpm1.6 and Tpm2.1 produces

101   opposite effects with respect to NM–2–dependent force development, with Tpm1.6 causing an

102   increase in intracellular pressure, whereas incorporation of Tpm2.1 decreases traction force

103   (Sao et al., 2019). In addition, Tpm2.1 has a specific role that other Tpm isoforms cannot

104   replace, supporting correct rigidity sensing and detection of tensile stress at the cell periphery

105   (Wolfenson et al., 2016). The incorporation of both LMW isoforms Tpm3.1 and 4.2 into stress

106   fibers promotes the specific recruitment of NM–2A (Bryce et al., 2003). Cofilaments formed

107   by F–actin and Tpm3.1 or Tpm4.2 are characterized by rapid dynamic exchange and are not

108   effectively protected from disassembly (Gateva et al., 2017). NM–2A was shown to have

109   increased sliding velocity and ATPase activity in complex with actin–Tpm3.1 (Barua et al.,

110   2014) and actin–Tpm4.2 cofilaments (Hundt et al., 2016). Moreover, the association of actin

111   filaments with Tpm3.1 or Tpm4.2 has been shown to increase ATP turnover by NM–2A and

112   NM–2B ATPase due to a specific acceleration of the rate–limiting step of phosphate release.

113   Under resisting force conditions, actin–Tpm3.1 and actin–Tpm4.2 cofilaments induce a slower

114   release of the hydrolysis product ADP, leading to an increase in duty–cycle and processive

115   behavior of NM–2B and NM–2A (Hundt et al., 2016; Pathan-Chhatbar et al., 2018).

116   In the case of cytoskeletal Tpm isoforms without N–terminal acetylation, apparent affinities

117   for filamentous actin in the range of 0.1 to 5 µM have been reported for Tpm1.6, Tpm1.7,

118   Tpm1.8, Tpm2.1, Tpm3. 1, and Tpm4.2. No clear correlation was found between affinity and

119   size of Tpm isoforms (Carman et al., 2021; Janco et al., 2016; Moraczewska et al., 1999; Ngo

120   et al., 2016). It is known that N–terminal acetylation is important for the ability of sarcomeric

121   Tpm isoforms to interact with F–actin, but less critical for the binding of the cytoskeletal Tpm

122   isoforms (Meiring et al., 2018; Palm et al., 2003). Biochemical and structural biology studies

123   suggest that N–terminal acetylation of Tpm isoforms not only acts locally but has consequences

124   for conformational dynamics far from the Tpm N–terminus and thus on the function and

125 stability of A–Tpm cofilaments (East et al., 2011; Greenfield et al., 1994; Johnson et al., 2018;

126 Monteiro et al., 1994; Palm et al., 2003). In the case of muscle–specific isoforms Tpm1.1 and

127 Tpm1.3, it was shown that the lack of N–terminal acetylation leads to an at least 30–fold lower

128 actin affinity (Heald and Hitchcock-DeGregori, 1988; Hitchcock-DeGregori and Heald, 1987).

129 Results available for Tpm3.1/3.2 and Tpm4.2 show that these cytoskeletal isoforms are almost

130 exclusively acetylated in primary and transformed human fibroblasts and epithelial cells

131 (Meiring et al., 2018). However, the precise impact of this post–translational modification on

132 actin binding by cytoskeletal Tpm isoforms and the functional properties of A–Tpm

133 cofilaments has remained unresolved. Further, N–terminal extensions consisting of 1 to 3

134 amino acid residues including Gly (Palm et al., 2003), Gly–Cys (Greenfield et al., 1994), Ala–

135 Ser (Monteiro et al., 1994; Palm et al., 2003), Ala–Ala–Ser (Monteiro et al., 1994), Lys–Met–

136 Thr (Heald and Hitchcock-DeGregori, 1988; Hitchcock-DeGregori and Heald, 1987), and Ala–

137 Ser–Arg (Urbancikova and Hitchcock-DeGregori, 1994) have been shown to restore the high

138 affinity actin binding of the muscle–specific isoforms Tpm1.1 and Tpm1.3 with little or no

139 interference with self–polymerization, myosin interactions and other regulatory functions

140 (Hitchcock-DeGregori and Heald, 1987; Maytum et al., 2000; Monteiro et al., 1994). As such,

141 these peptide extensions, but especially the Ala–Ser dipeptide, are now widely used as N–

142 terminal acetylation mimics for the production of recombinant muscle–specific as well as

143 cytoskeletal Tpm constructs (Coulton et al., 2006; Palm et al., 2003).

144 Considering the essential functions of actomyosin complexes in non–muscle cells and the

145 almost complete association of cytoskeletal F–actin with Tpm cables (Meiring et al., 2018), it

146 is of paramount importance to elucidate the contribution of Tpm cables to contractile processes

147 by investigating the influence of their isoform composition, exon usage, and N–terminal

148 acetylation (Arnesen et al., 2009; Silva and Martinho, 2015). Here, we describe how the

149 activities of the cytoskeletal myosin isoforms Myo1C[0] (Adamek et al., 2008; Giese et al., 2020;

150 Zattelman et al., 2017), NM–2A (Kovács et al., 2003; Müller et al., 2013), and myosin–5A (De

151 La Cruz et al., 1999; Mehta et al., 1999; Rock et al., 2000), which exert distinct enzymatic

152 properties and cellular functions, are regulated by different Tpm isoforms and how N–terminal

153 Tpm acetylation influences the functional properties of these myosin isoforms. We show by

154 biochemical analysis of reconstituted A–Tpm–M complexes that the motor activity of human

155 Myo1C[0], NM–2A, and myosin–5A are each regulated in different ways by Tpm isoforms, and

156 that N–terminal acetylation of Tpm alters this regulation to a significant extent and in a manner

157 specific to each myosin isoform.

158

159 **RESULTS**

160 **Expression, purification and initial characterization of proteins for the in vitro**
161 **reconstitution of physiological A–Tpm–M complexes**

162 To characterize the functional properties of cytoskeletal A–Tpm cofilaments and their
163 interactions with myosin motors, we produced and purified the human isoforms of β–actin, γ–
164 actin, tail truncated versions of Myo1C isoform C^0 (Myo1C^0–ΔTH1), and heavy meromyosin
165 (HMM)–like constructs of NM–2A and myosin–5A in active and soluble forms using the
166 SF9/baculovirus system. In humans, alternative splicing of the *MYO1C* gene leads to the
167 production of three isoforms, which differ in the length of their N–terminal extensions
168 (Ihnatovych et al., 2012; Nowak et al., 1997). Compared to Myo1C^0, the isoforms Myo1C^{16}
169 and Myo1C^{35} contain 16 and 35 additional amino acids at their N–terminus. Typically, we
170 obtained up to 3.5 mg of the cytoskeletal actin isoforms, 1.6 mg Myo1C^0–ΔTH1, 0.6 mg NM–
171 2A–HMM, and 0.5 mg myosin–5A–HMM per 1 liter of culture medium.

172 Human Tpm isoforms were produced in *E. coli* BL21(DE3) for the non–acetylated isoforms
173 and for the acetylated isoforms in *E. coli* BL21(DE3) cells coproducing either the fission yeast
174 NatA or NatB complex. The sequential induction of the appropriate Nat complex, followed by
175 expression and repression of the respective Tpm isoform of interest, has been shown to result
176 in near complete N–terminal acetylation (Eastwood et al., 2017). Additionally, the presence of
177 N–terminal acetylation was probed for isoforms derived from *TPM1* and *TPM2* using
178 antibodies recognizing either the acetylated or non–acetylated Tpm N–terminus (Figure 2A).
179 Both the non–acetylated and acetylated Tpm isoforms were purified to homogeneity in yields
180 of 15–20 mg per liter. Previous work from our laboratory has shown significant differences in
181 the ability of isoactins to bind and stimulate the enzymatic activity of human NM–2A, –2B, –
182 2C and myosin–7A. In the case of NM–2A and –2B, the interaction with either cytoplasmic
183 actin isoform results in 4–fold greater stimulation of myosin ATPase activity than was
184 observed in the presence of α–skeletal muscle actin (Müller et al., 2013). Significant
185 differences were also observed in initial control experiments performed for the interaction of
186 human myosin–5A with the different isoactins. Accordingly, all subsequently described
187 experiments using NM–2A and myosin–5A constructs were performed with cytoskeletal β–
188 actin. The situation is different for Myo1C, where we observed no significant change in ATP
189 turnover and motile activity upon exchange of the actin isoform (Supplemental figure 1 A, B).
190 Likewise, we observed comparable maximal inhibition of 40 ± 5% and IC$_{50}$ values of 3.5 ±
191 0.3 µM for ATP turnover by acto–Myo1C^0–ΔTH1 in the presence of Tpm3.1 and AcTpm3.1.

192   Therefore, all experiments involving Myo1C^0–ΔTH1 were performed using α–actin and non–

193   acetylated Tpm isoforms.

194   To investigate the effects of exon usage 1a.2b in HMW–Tpm isoforms compared to 1b in LMW

195   isoforms, as well as the importance of internal exon 6a compared to 6b, we performed

196   cosedimentation tests with β–actin in combination with HMW–Tpm isoforms 1.6 and 2.1 or

197   LMW isoforms 3.1 and 4.2. Myo1C motor functions were studied in detail in complex with

198   Tpm1.7 and Tpm3.1 as *in vivo* and *in vitro* studies provide clear evidence for the role of Tpm1.7

199   and Tpm3.1 decorated actin cytoskeleton in the regulation of Myo1C localization at specific

200   cell sites and motor functions (Kee et al., 2015; McIntosh et al., 2015; Pelham et al., 1996).

201   We observed values for half–maximal saturation of binding ($K_{50\%}$) in a narrow range between

202   1.3 and 2.0 µM with the HMW isoforms Tpm1.6 and Tpm2.1 and the LMW isoforms Tpm3.1,

203   and Tpm4.2 (Figure 2C). Each of these isoforms is prominently associated with stress fibers in

204   a variety of human cell types (Gateva et al., 2017). Tpm isoforms included in our study that

205   are typically not associated with stress fibers such as Tpm1.8 and Tpm1.12 have $K_{50\%}$ values

206   that lie outside this narrow range. Approximately 10–fold higher and lower apparent binding

207   affinities were observed with Tpm1.8 and Tpm1.12, respectively (Table 1).

Impact of N–terminal Tpm acetylation on interaction with filamentous actin

209   Following N–terminal acetylation, we observed only minor changes in the $K_{50\%}$ for filamentous

210   β–actin, with increases in apparent binding affinity for the N–acetylated forms from 1.32 to

211   1.23 µM for Tpm1.6, 1.50 to 1.15 µM for Tpm3.1, and 1.99 to 1.33 µM for Tpm4.2. The

212   opposite effect was observed upon acetylation for Tpm1.12 and Tpm2.1, resulting in a decrease

213   in apparent binding affinity from 18.2 to 28.8 µM and 1.73 to 2.29 µM, respectively (Figure

214   2C, Table 1). At least in the absence of other actin–binding proteins, our results support the

215   view that there exists no direct relationship between the F–actin binding affinities of

216   cytoskeletal Tpm isoforms and molecular weight (Carman et al., 2021; Janco et al., 2016;

217   Moraczewska et al., 1999; Ngo et al., 2016). Our results show in addition that N–terminal

218   acetylation has only a minor impact on the actin affinity of cytoskeletal Tpm isoforms, again

219   without clear correlation to size.

220   Next, we investigated whether the thermal stability of A–Tpm cofilaments is altered by N–

221   terminal acetylation. In agreement with previous data obtained using smooth muscle isoforms

222   (Levitsky et al., 2000), we show that the dissociation of cytoskeletal Tpm isoforms from

223   filamentous β–actin is reversible and shows pronounced hysteresis, with dissociation occurring

224   at higher temperatures than reassociation (Figure 2D). A comparison of T_{diss} for non–acetylated

7

225   and acetylated Tpm1.6, Tpm2.1, Tpm3.1 and Tpm4.2 revealed significant isoform–specific

226   differences in dissociation properties (Figure 3A–D, Table 1). Specifically, in the absence of

227   N–terminal acetylation, the HMW isoforms Tpm1.6 and Tpm2.1 display higher T_{diss} values of

228   41.2° and 38.0°C than the LMW isoforms Tpm3.1 and Tpm4.2 with T_{diss} values of 35.6° and

229   36.5°C. In the case of the HMW isoforms, N–terminal acetylation leads to a slight reduction

230   of T_{diss}. In contrast, the LMW isoforms show marked stabilization of their cofilaments with F–

231   actin by 9 °C or more after N–terminal acetylation. In the case of Tpm4.2, N–terminal

232   acetylation shifts the light scattering signal into the range where denaturation of F–actin starts

233   to occur, the observed processes become irreversible, and dissociation cannot be fully resolved

234   (Figure 3D, Table 1). In line with previous studies (Levitsky et al., 2000), we observed that the

235   T_{diss} values measured for the different acetylated and non–acetylated isoforms depend strongly

236   on Tpm concentration. Secondary plots of T_{diss} against the total Tpm concentration are well–

237   described by hyperbolas. N–terminal acetylation of Tpm 1.6 resulted in small increases in T_{diss}

238   over the entire concentration range. A much stronger stabilization of cofilaments was observed

239   after N–terminal acetylation of Tpm3.1, evident from a marked leftward shift and an

240   approximately 10°C higher plateau value of the hyperbola (Figure 3E–F).

241   **Modulation of actin–activated ATPase and motor activity of myosin–1C[0] by cytoskeletal**
242   **Tpm isoforms**

243   The actin–activated steady–state ATPase activities of Myo1C[0]–ΔTH1 were determined with

244   10 µM A–Tpm cofilaments composed of α–actin and non–acetylated LMW isoforms Tpm3.1,

245   Tpm4.2 or HMW isoforms Tpm1.6, Tpm1.7. Marked reductions in ATP turnover of Myo1C[0]–

246   ΔTH1 were observed in the presence of all Tpm isoforms tested (Figure 4A). It should be noted

247   that the ATPase rates reported in Table 2 refer to values obtained at a sub–saturating

248   concentration of 10 µM A–Tpm cofilaments and thus cannot be directly compared with the

249   values obtained at saturating concentrations of bare F–actin and Tpm cofilaments. The actin–

250   activated steady–state ATPase activities of Myo1C[0]–ΔTH1 in the absence and presence of

251   HMW isoform Tpm1.7 or LMW isoform Tpm3.1, were determined at actin concentrations

252   ranging from 0 to 50 µM. Under both conditions, we observed a reduction in maximum ATP

253   turnover of approximately 33% for Myo1C[0]–ΔTH1 (Table 2). We used stopped–flow kinetics

254   to determine the impact of HMW Tpm1.7 and LMW Tpm3.1 on the binding of Myo1C[0]–ΔTH1

255   to F–actin in the absence of nucleotide, ATP–induced dissociation of Myo1C[0]–ΔTH1 from F–

256   actin, ADP affinity of acto–Myo1C[0]–ΔTH1, and the release of the hydrolysis products

257   phosphate and ADP. The results of these measurements are summarized in Table 3. They show

258   a significant reduction in the rate constant for phosphate release (k_{+4}) from 0.09 ± 0.01 s^{-1} in

8

259 the presence of bare F–actin to 0.07 ± 0.01 s^{-1} in the presence of cofilaments containing either

260 Tpm1.7 or Tpm3.1. We have previously shown that in the presence of bare F–actin k_{cat}, the

261 maximum value of ATP turnover in the presence of saturating actin concentrations, is reduced

262 from ~0.37 s^{-1} at 37°C to 0.09 ± 0.02 s^{-1} at 20°C (Giese et al., 2020). Thus, in the absence and

263 presence of Tpm isoforms, the observed differences between the rate limiting step k_{+4} and k_{cat}

264 are primarily due to the different temperatures at which the transient and steady–state kinetics

265 experiments were performed. The impact of the Tpm isoforms on the rate of ADP release from

266 Myo1C^0–ΔTH1 was determined by ATP–induced dissociation of the actomyosin complex

267 (Geeves, 1989). The active sites of 0.5 µM Myo1C^0–ΔTH1 were saturated with 20 µM ADP,

268 so that ATP binding is rate–limited by the slow dissociation of ADP. The transients were best–

269 fitted with a single exponential function yielding rate constants for ADP release (k_{+5}) that are

270 30 and 34% slower for cofilaments containing Tpm1.7 (1.11 ± 0.09 s^{-1}). and Tpm3.1 ($1.05 \pm$

271 0.05 s^{-1}) than the rate constant obtained with bare F–actin (1.59 ± 0.07 s^{-1}). Finally,

272 measurements of the ATP–induced dissociation of pyrene–labeled acto–Myo1C^0–ΔTH1

273 revealed a significant change in the equilibrium constant for isomerization of the nucleotide

274 binding pocket K_α indicating a shift towards greater occupancy of states with closed nucleotide

275 binding pocket in the presence of cofilaments containing Tpm1.7 or Tpm3.1.

276 To determine the influence of A–Tpm cofilaments on myosin–1C motor function, we

277 performed *in vitro* motility assays. No motile activity was detectable on Myo1C^0–ΔTH1–

278 decorated surfaces, when bare actin filaments were replaced with A–Tpm cofilaments under

279 the standard conditions of the *in vitro* motility assay. Titrations of the Myo1C^0–ΔTH1surface

280 density showed that the minimum motor density to achieve a stable plateau value for

281 continuous directional movement increased from 900 motors µm^{-2} with bare F–actin to >4,000

282 motors µm^{-2} in the presence of A–Tpm cofilaments (Supplemental figure 2). Compared with

283 the plateau value of 52.1 ± 4.9 nm s^{-1} obtained for filament sliding velocity with bare F–actin

284 on lawns of Myo1C^0–ΔTH1, approximately 5.5–fold slower values were observed in the

285 presence of Tpm1.6, Tpm1.7, Tpm1.12, Tpm2.1, Tpm3.1, and Tpm4.2 (Table 2). Based on

286 results obtained with class–2 myosins (Greene and Eisenberg, 1980; Ngo et al., 2016), we

287 expected the cytoskeletal Tpm isoforms and Myo1C^0 to mutually strengthen each other's

288 affinity for F–actin in the presence of ATP. With NM–2B, we had observed a change in the

289 $K_{50\%}$ for F–actin binding by Tpm1.12 from ≥40 µM to <1 µM (12). However, when we

290 replaced NM–2B with Myo1C^0, a much smaller increase in the apparent actin affinity of

291 Tpm1.12 ($K_{50\%} = 19.3 \pm 1.1$ µM) was recorded. The reduced mutual cooperative enhancement

292 of actin binding by the cytoskeletal Tpm isoforms and Myo1C^0 is clearly evident in the dose–

293   response curves for inhibition of Myo1C^0–supported motile activity by the various cytoskeletal

294   Tpm isoforms (Figure 4B). Tpm2.1 showed a similar 2–fold change in $K_{50\%}$ in the presence of

295   Myo1C^0. Smaller changes were recorded for cofilaments containing Tpm3.1 and Tpm4.2 in

296   the presence of Myo1C^0, with increases in $K_{50\%}$ of 13 and 25%, respectively (Table 1).

297   To analyze the influence of the distinct Tpm isoforms on Myo1C–driven force development,

298   we determined the ability of Myo1C^0–ΔTH1 to translocate A–Tpm cofilaments in the presence

299   of an external load using frictional loading experiments (Greenberg and Moore, 2010). Binding

300   of surface–attached α–actinin to A–Tpm cofilaments leads to a reduction in the filament sliding

301   velocity as the external load increases with the concentration α–actinin and impedes the driving

302   force of myosin (Figure 4C). We have previously observed that the load–dependent changes in

303   the sliding velocities of Myo1C^0–ΔTH1 are best described by a tension–sensing mechanism

304   that includes a force–dependent and a force–independent transition (Giese et al., 2020). The

305   resulting force–velocity dependences (Figure 4D) indicate a marked reduction in motive power

306   generation in the presence of actin cofilaments containing Tpm1.7 or Tpm3.1.

307   **Modulation of actin–activated ATPase and motor activity of non–muscle myosin–2A and**
308   **myosin–5A by non–acetylated cytoskeletal Tpm isoforms**

309   The observed maximum actin–activated ATPase activity of NM–2A with bare filamentous β–

310   actin ($k_{cat} = 0.26 \pm 0.02$ s^{-1}) is in good agreement with published data (Hundt et al., 2016;

311   Kovács et al., 2003). Functional assays performed with NM–2A in the presence of saturating

312   concentrations of non–acetylated HMW tropomyosin isoforms Tpm1.6 and Tpm2.1 and LMW

313   isoforms Tpm3.1 and Tpm4.2 show isoform–specific variations in catalytic activity. The

314   strongest effect was observed for Tpm3.1, with a 2.5–fold increase in k_{cat} and 63% faster

315   velocity compared to bare F–actin. Cofilaments containing Tpm2.1 showed a 1.5–fold increase

316   in k_{cat} and a 12% faster velocity. In the case of Tpm1.6 and Tpm4.2, we observed a 34% and

317   42% increase in k_{cat} together with smaller changes in velocity, which are within the margin of

318   error of our assay (Figure 5A,B; Table 2).

319   Assays performed with myosin–5A in the presence of saturating concentrations of non–

320   acetylated Tpm1.6, Tpm2.1, Tpm3.1 and Tpm4.2 show reductions in actin–activated ATP

321   turnover and sliding velocities ranging from 28 to 42 % compared to bare F–actin (Figure

322   6A,B; Table 2). In contrast, cofilaments containing Tpm1.12 move approximately 12% faster

323   than bare F–actin at a myosin–5A–HMM surface density corresponding to approximately 18

324   double–headed motor molecules per µm^2. ATP turnover by myosin–5A was not significantly

325   affected by cofilaments containing Tpm1.12. With respect to the run length of filaments, we

326   observed a significant reduction for cofilaments containing Tpm1.12 and a significant increase

327   for those containing Tpm4.2. The run length of cofilaments containing Tpm1.6, Tpm2.1, or

328   Tpm3.1 was unchanged compared to bare filamentous β–actin (Supplemental figure 3). Similar

329   protection of filaments from fragmentation was observed for all Tpm isoforms tested.

330   **Impact of N–terminal Tpm acetylation on actin–activated ATPase and motor activity of**
331   **NM–2A and myosin–5A**

332   For the HMW isoforms Tpm1.6 and Tpm2.1, only minor differences in the k_{cat} of NM–2A

333   were observed between the acetylated and non–acetylated forms of the proteins. The observed

334   changes in the concentration required for half–maximal activation of ATP turnover (K_{app}) are

335   within the margin of error of our assay (Figure 7A,B). Larger opposing effects were observed

336   for NM–2A in the presence of saturating concentrations of A–Tpm cofilaments containing

337   either the acetylated or non–acetylated forms of LMW Tpm3.1 and Tpm4.2. Cofilaments

338   containing Tpm3.1 show a 2.5–fold increase in k_{cat} (0.26 s^{-1} versus 0.64 s^{-1}), while K_{app} is

339   reduced 1.4–fold and k_{cat}/K_{app} is more than 3.6–fold increased in the presence of Tpm3.1. These

340   are the strongest effects observed for a non–acetylated Tpm isoform (Figure 7C). N–terminal

341   acetylation of Tpm3.1 reduces the increase in k_{cat}/K_{app} to 2.2–fold, together with corresponding

342   changes in k_{cat} and K_{app}. In the case of Tpm4.2, N–terminal acetylation has the opposite effect

343   than that observed with Tpm3.1. The calculated k_{cat} is increased 1.6–fold for AcTpm4.2 from

344   0.37 to 0.61 s^{-1} and k_{cat}/K_{app} increases 2.1–fold from 1.12×10^{-2} to 2.34×10^{-2} $\mu M^{-1}s^{-1}$ in the

345   presence of AcTpm4.2 (Figure 7D).

346   AcTpm1.6, AcTpm2.1, AcTpm3.1, and AcTpm4.2 containing cofilaments move

347   approximately 53, 21, 63, and 43% faster on lawns of NM–2A than bare F–actin (Figure 7E).

348   While k_{cat} is reduced by 25% in the presence of AcTpm3.1 compared to Tpm3.1, both Tpm3.1

349   and AcTpm3.1 containing cofilaments move on lawns of NM–2A with the same velocity and

350   approximately 63% faster than bare F–actin. With this exception all other cofilaments

351   containing AcTpm isoforms move faster than cofilaments containing the non–acetylated Tpm

352   isoforms. In the case of Tpm2.1 and Tpm4.2, the changes in motor activity observed upon N–

353   terminal acetylation correspond to the trend observed in ATP turnover measurements.

354   Following N–terminal acetylation, similar increases in both parameters were observed for

355   Tpm2.1 (<8%) and Tpm4.2 (>40%). In contrast, N–terminal acetylation of Tpm1.6 results in

356   a 35% increase in sliding velocity but a 11% decrease in k_{cat} (Figure 7; Table 2).

357   In the case of myosin–5A, the differences in unloaded velocity, event frequency and run length

358   between acetylated and nonacetylated Tpm isoforms are mostly within the margin of error,

359   with the following exceptions. Cofilaments containing Tpm1.12 move significantly faster on

360   lawns of myosin–5A–HMM than bare filamentous β–actin and cofilaments containing

361   AcTpm1.12 (Figure 8; Table 2). The percentage of filaments showing unidirectional uniform

362   motion on lawns of myosin–5A–HMM was equal and higher than 98% for bare filaments and

363   all cofilaments studied. Similar protection of filaments from fragmentation was observed for

364   the acetylated and nonacetylated Tpm isoforms. The run length of cofilaments containing

365   AcTpm1.6 or AcTpm3.1 was unchanged relative to bare filamentous β–actin and cofilaments

366   containing the nonacetylated Tpm isoforms. Cofilaments containing Tpm2.1 showed a small

367   but significant increase in run length that was not observed for AcTpm2.1. The run lengths of

368   cofilaments containing Tpm4.2 and AcTpm4.2 were 8% and 12% longer, while those of

369   cofilaments containing Tpm1.12 or AcTpm1.12 were approximately 15% and 20% shorter,

370   respectively (supplemental Figure 3).

371

372   **DISCUSSION**

373   *Actin–Tpm interactions*

374   Myosin–induced contraction has long been studied in skeletal and cardiac muscle, where thin

375   actin filaments move along thick myosin filaments and actomyosin–based motility is regulated

376   by Tpm–dependent cooperative on–off switching, which is mediated by the binding of Ca^{2+} to

377   the troponin–C subunit of the troponin–Tpm complex on thin filaments (Greaseri and Gergely,

378   1971). Binding of Tpm to F–actin has been extensively characterized for the muscle isoforms

379   and more recently also for individual cytoskeletal Tpm isoforms (Marchenko et al., 2021;

380   Maytum, Konrad, Lehrer, & Geeves, 2001; Pathan–Chhatbar et al., 2018; Schmidt, Lehman,

381   & Moore, 2015). Emerging experimental results and molecular dynamics simulations support

382   a form–function relationship that has been referred to as Gestalt–binding (Holmes and Lehman,

383   2008; Lehman et al., 2019).

384   Gestalt–binding allows global changes in the position of Tpm cables as well as local positional

385   perturbations caused by troponin, myosin or other actin–binding proteins and gives the A–Tpm

386   cofilaments sufficient flexibility to allow alternative binding modes at low energy cost, while

387   promoting tight cooperative coupling that is highly sensitive to allosteric trigger events such

388   as post–translational modifications, protein–protein interactions, ligand binding or isoform–

389   specific amino acid substitutions (Fischer et al., 2016; Holmes and Lehman, 2008; Li et al.,

390   2010). This provides the cell with a toolbox of modular components consisting of cofilaments

391   containing different Tpm isoforms with and without post–translational modifications, capable

392   of acting as mechanical sensors, selective tracks for myosin motors and ultrasensitive switches.

393 As mediators between chemical and mechanical signal transduction pathways, they enable cells

394 to carry out precisely tuned reactions. The characterization of such systems requires an

395 approach that incorporates accurate allosteric awareness overcoming difficulties in producing

396 the correct combinations of protein isoforms with relevant post–translational modifications for

397 the accurate determination of rate and equilibrium constants, structural features, forces, and

398 velocities (Preller and Manstein, 2013). Therefore, we used contractile filaments composed of

399 human cytoskeletal actin, myosin, and Tpm isoforms and produced the recombinant proteins

400 without introducing any changes to their native sequence. Amino–terminally acetylated Tpm

401 isoforms were produced in bacteria rather than the commonly used isoforms carrying a short

402 N–terminal extension, such as Ala-Ser, to mimic acetylation. Phalloidin labelled with

403 tetramethyl–rhodamine B isothiocyanate was used exclusively to stabilize and stain F–actin for

404 *in vitro* motility assays, but omitted from all other assays.

405 Apart from the influence of post–translational modifications, Tpm binding to actin has been

406 reported to be primarily dependent on exon usage (Cho and Hitchcock-DeGregori, 1991;

407 Moraczewska et al., 1999; Pathan-Chhatbar et al., 2018; Schmidt et al., 2015). Variable exons

408 1 and 9, which specify residues contributing to the Tpm overlap complex, have been shown to

409 affect actin affinity in the order 1b9d>1b9a>Ac1a9a>1a9d≫1a9a≧1a9c≅1b9c in the context

410 of recombinant Tpm1.3 smooth muscle variants that are identical except for the terminal

411 regions encoded by exons 1a or 1b and exons 9a, 9c or 9d (Pathan-Chhatbar et al., 2018). Exon

412 1a is expressed in muscle and non–muscle cells, while exon 1b replaces exons 1a and 2 in non–

413 muscle cells, resulting in the production of LMW Tpm isoforms. The C–terminal exon 9a is

414 expressed in striated muscles, endothelial cells, and in the brain, exon 9c exclusively in the

415 brain, and exon 9d in non–muscle as well as in smooth muscle cells (Dufour et al., 1998;

416 Schevzov et al., 2011; Vrhovski et al., 2003). Our results show for cytoskeletal Tpm isoforms

417 that sequences contributing to the overlap region are not the sole determinant of differences in

418 actin affinity. Changes for the non–acetylated LMW isoforms range from Tpm1.8(b.–.b.d;

419 $K_{50\%}$: 0.10 μM), Tpm3.1(b.–.a.d; $K_{50\%}$: 1.50 μM), Tpm4.2(b.–.b.d; $K_{50\%}$: 1.99 μM), to

420 Tpm1.12(b.–.b.c; $K_{50\%}$: ≥40 μM). The HMW isoforms Tpm1.6(a.b.b.d; $K_{50\%}$: 1.32 μM) and

421 Tpm2.1(a.b.a.d; $K_{50\%}$: 1.73 μM) display actin affinities similar to the LMW isoforms Tpm3.1

422 and Tpm4.2. Regarding the role of variable exon 6 in shaping Tpm diversity in terms of A–

423 Tpm interactions and cofilament mechanical properties, a comparison of LMW isoforms

424 Tpm3.1(b.–.a.d) and Tpm4.2(b.–.b.d) and the HMW isoforms Tpm1.6(a.b.b.d) and

425 Tpm2.1(a.b.a.d) shows that global sequence differences between the four *TPM* genes are of

426 greater importance than variable exon 6 usage. Moreover, the differences that can be attributed

13

427 to exon 6 usage are comparable in extent to those mediated by the presence or absence of N–

428 terminal acetylation. The weakest binding to F–actin was observed with the use of exon 9c by

429 Tpm1.12(b.–.b.c).

430 Our investigations of the temperature–dependent dissociation and reassociation of human

431 cytoskeletal A–Tpm cofilaments revealed Tpm isoform–specific differences in T_{diss}, as well as

432 differences in the extent of hysteresis exhibited by the dissociation and reassociation reactions,

433 and the effects of N–terminal acetylation. While in the absence of N–terminal acetylation the

434 T_{diss} values of the HMW isoforms Tpm1.6 and Tpm2.1 exceeded those measured for the LMW

435 isoforms Tpm3.1 and Tpm4.2 by 1° to 6°C, the opposite was true for the isoforms with N–

436 terminal acetylation. Compared to an increase of T_{diss} by 10° to 13°C upon acetylation of

437 Tpm3.1 and Tpm4.2, acetylation of Tpm1.6 and Tpm2.1 leads to a reduction of T_{diss} by 1° to

438 2°C. In line with the kinetic binding model of Tpm molecules to actin (Bareja et al., 2020),

439 greater thermal stability of A–Tpm can be explained by stronger end–to–end contacts of Tpm

440 molecules. Alternative explanations include stronger coordination of Tpm assembly on actin

441 filaments or greater flexibility of Tpm cables. Both lead to changes in gap formation, which

442 have been described as sites of dissociation (Orzechowski et al., 2014; Schmidt et al., 2015).

443 The number of gaps is thought to be controlled by Tpm concentration (Schmidt et al., 2015),

444 which is consistent with our observation that changes in Tpm concentration affect the size of

445 cooperative units. Gap formation potentially provides an additional selectivity filter for Tpm–

446 gated access of actin–binding proteins to cytoskeletal F–actin. This is evident from differences

447 in the exchange of free Tpm3.1 and Tpm4.2 with Tpm isoforms bound to F–actin. The much

448 stronger effect of N–terminal acetylation on the temperature stability of A–Tpm containing

449 LMW–Tpm isoforms compared with HMW–Tpm isoforms suggests that changes within the

450 overlap region of Tpm cables lead to analogous differences in allosteric communication.

451 A comparison of our results obtained with the acetylated and non–acetylated isoforms of

452 Tpm1.6, Tpm1.12 and Tpm4.2 (Table 1) and the reported T_{diss} and $K_{50\%}$ values for the

453 corresponding Ala-Ser–tagged isoforms reveals minor changes (Marchenko et al., 2021). Thus,

454 Ala–Ser labeling may have an influence on allosteric communication and cooperative coupling

455 in A–Tpm cofilaments that remains to be confirmed, but is not required for efficient binding

456 of these cytoskeletal Tpm isoforms to F–actin.

457 *Functional diversification of cytoskeletal A–Tpm cofilaments and A–Tpm–M complexes*

458 Tpm–specific regulation of cytoskeletal myosin isoforms has been described as being

459 dependent on the myosin isoform or myosin class involved (Barua et al., 2014; Clayton et al.,

14

460   2015, 2014; Kee et al., 2015; Pathan-Chhatbar et al., 2018). It has been proposed that A–

461   Tpm3.1 cofilaments limit or block motor function, allowing Myo1C to perform its cellular

462   functions only in areas containing bare actin filaments (Kee et al., 2015). In the presence of

463   cytoskeletal A–Tpm cofilaments including A–Tpm3.1, our results show up to 80 % slower

464   sliding velocities, a 27 to 38% decrease in k_{cat} and marked reductions in force generation.

465   However, as the apparent affinity of Myo1C for F–actin in the presence of ATP (K_{app}) remains

466   unchanged in the presence of saturating concentration of cytoskeletal Tpm isoforms, we favor

467   a role for the cytoskeletal A–Tpm cofilaments where they interact productively with human

468   Myo1C by shifting motor activity from faster movement on bare F–actin to more efficient

469   tension sensing on A-Tpm cofilaments. Such a shift is consistent with the distinct roles of

470   Myo1C in transport, storage, and insertion of GLUT4 vesicles into the plasma membrane

471   (Boguslavsky et al., 2012).

472   Based on event frequency, run length, and unloaded velocity, actin–Tpm3.1 and actin–Tpm1.8

473   cofilaments were described as equal or better tracks compared to bare actin for murine myosin

474   5A–HMM. In contrast, actin–Tpm4.2 was described to exclude myosin 5A–HMM from

475   productive interactions (Sckolnick, Krementsova, Warshaw, & Trybus, 2016). Our results

476   show more subtle changes supporting graded functional adjustments as consequence of an

477   exchange of Tpm isoform. Under the experimental conditions used, both the rate of ATP

478   turnover and the sliding velocity supported by human myosin–5A show significant reductions

479   for most tested cytoskeletal Tpm isoforms with and without N–terminal acetylation. The

480   exception is Tpm1.12 showing a significant increase in sliding velocity. Taking also into

481   account the observed changes in run lengths, a uniformly high event frequency for all

482   cofilament combinations examined, and the limitations of the assays used, we conclude that

483   our results are dominated by a cofilament–specific modulation of the myosin–5A duty ratio.

484   Therefore, exactly how motile and contractile activities play out in a cellular environment will

485   depend on several other parameters, including local variations in motor density, external load,

486   spatial constraints, and the presence of actin–binding auxiliary proteins.

487   Unlike the two other myosin isoforms tested, NM–2A shows increased enzymatic activity in

488   the presence of most of the A–Tpm cofilaments tested. The extent of the enhancement of

489   ATPase activity and sliding velocity varied for the different Tpm isoforms as well as with their

490   N–terminal acetylation status. The largest changes in ATP turnover kinetics and the fastest

491   sliding velocities were observed for A–Tpm cofilaments containing either Tpm3.1 or

492   AcTpm3.1. Cofilaments containing AcTpm1.6 and AcTpm4.2 moved significantly faster

493   compared to the non–acetylated isoforms and bare F–actin. Cofilaments containing AcTpm2.1

494   displayed a small but significant increase in velocity only over bare F–actin. These findings

495   provide a more nuanced picture compared with the previously reported enhanced NM–2A–

496   dependent motor activity of A–Tpm cofilaments containing LMW Tpm3.1 and Tpm4.2 and a

497   reduced productive interaction of cofilaments containing HMW Tpm1.6 and Tpm2.1 with

498   NM–2A (Gateva et al., 2017). Inclusion of the N–terminally acetylated isoforms increase the

499   physiologically relevance of our results.

500   Collectively, our ensemble kinetics values provide accurate descriptions of the effects of Tpm

501   isoform exchange or changes in Tpm–acetylation status on the maximum rate of ATP turnover,

502   the apparent affinity for the filament track in the presence of ATP, and the strength of the

503   coupling between binding to filament tracks and the acceleration of rate–limiting steps in the

504   actomyosin ATPase cycle. Opposing changes in the catalysis of ATP turnover and motor

505   activity can be attributed to isoform–specific allosteric coupling between the different

506   components of A–Tpm–M complexes that is responsive to the extent of saturation at which the

507   solution kinetics and *in vitro* motility experiments are performed and to the surface density and

508   arrangement of myosin motors in the *in vitro* motility assays (Hundt et al., 2016; Pertici et al.,

509   2018; Toyoshima et al., 1989; Uyeda et al., 1990). Our results show how motor properties such

510   as maximum velocity in the absence and presence of external loads and optimal motor density

511   for continuous unidirectional motion, previously considered specific and invariant properties

512   of each myosin isoform, are modulated by the presence of different Tpm isoforms as well as

513   their post–translational modification. This provides a solid and indispensable foundation for

514   future studies aimed at discovering small molecule therapeutics for the treatment of non–

515   muscular myosinopathies and actinopathies.

516   **LIMITATIONS OF THE STUDY**

517   The scope of our study is limited by the allosteric nature of the system under investigation,

518   with the existence of a large number of possible combinations of cytoskeletal actin, myosin,

519   and Tpm isoforms. Our study is focused on the *in vitro* characterization of selected A–Tpm–

520   M combinations. The examples presented in our work reveal important key aspects for the

521   major isoforms. In addition, they define the range over which the functional properties of A–

522   Tpm–M complexes typically vary, and they allow certain combinations of isoforms to be

523   clustered into groups with similar properties. Overall, our work provides a starting point and

524   framework for quantitative modelling of motor processes at the cellular level. To realize its full

525 potential, further studies are needed that provide insights into the subcellular localization of
526 related motor processes, the spatial distribution, density and concentration of the individual
527 components, and the impact of posttranslational modifications on their functional properties.

528 **ACKNOWLEDGEMENTS**

541

542 **AUTHOR CONTRIBUTIONS**

543 All authors discussed the results and contributed to the final manuscript; T.R. and S.G. purified
544 proteins, performed experiments; T.R., S.G., J.N.G. and D.J.M. analyzed data; T.R., S.G., and
545 D.J.M. designed the figures; T.R., S.G., J.N.G., D.P.M., I.C., M.H.T. P.Y.R., and S.L.L.
546 contributed to the experimental design, data interpretation and manuscript preparation; T.R.
547 and D.J.M. wrote the manuscript; D.J.M. conceived and coordinated the study, was responsible
548 for funding acquisition and project administration.

549

550 **DECLARATION OF INTERESTS**

551 The authors declare no competing interests.

552

553 **INCLUSION AND DIVERSITY**

554 While citing references scientifically relevant for this work, we also actively worked to
555 promote gender balance in our reference list.

556 **FIGURES**

557 **Figure 1: Schematic representations of exon usage for selected Tpm isoforms and the**

558 **functional context of selected myosin isoforms.** (A) Exon usage for Tpm1.6, Tpm1.7,

559 Tpm1.8, Tpm1.12 Tpm2.1, Tpm3.1and Tpm4.2. Black boxes represent constitutively

560 expressed exons, grey regions represent alternatively spliced coding regions and non–coding

561 regions are shown as white boxes. (B)–(E) Myosin family motor proteins consist of a generic

562 motor domains (green) followed by a lever arm with light chain binding sites (orange) and the

563 tail region (blue). (B) Class 1 myosins act in part by connecting membrane lipids with the actin

564 cytoskeleton. They support short range vesicle transport, modulate actin assembly and

565 function, act as the adaptation motor in the stereocilia of the inner ear, and are implicated in

566 transcription regulation. (C) The actomyosin ATPase cycle, which is shared by all myosin

567 classes with the exception of class 18, includes the rigor state (state A) and progresses via the

568 following transitions: ATP binding (A→B; K_1), dissociation of the actomyosin complex

569 (B→C; K_2), ATP hydrolysis (C→D; K_3), reassociation with formation of a weak actomyosin

570 complex (D→E, K_9), phosphate release, formation of a strong actomyosin complex and

571 powerstroke (E→F; K_4), ADP release (F→A; K_5), which returns the Myo1C to the rigor state.

572 (D) Non–muscle myosin–2 isoforms are predominantly organized into stress fibres, which are

573 able to generate contractile forces that support functions such as cell adhesion, migration and

574 mechanotransduction. (E) Class 5 myosin dimers act in part by transporting cargo such as

575 vesicles from the centre of the cell towards the periphery. The polarity of the actin filament is

576 indicated as +(barbed) and –(pointed) ends.

577

578 **Figure 2: Interaction of distinct Tpm isoforms with actin and impact of the actin isoform**

579 **used in functional assays.** (A) Blot of non–acetylated and acetylated Tpm1.6 and Tpm2. 1

580 immunostained either with sheep polyclonal antibody Millipore AB5441 directed against

581 isoforms containing a region encoded by exon 9d of *TPM1* or *TPM2* (left panel) or with rabbit

582 polyclonal antibody D55Ac directed against the N–acetylated forms of gene products encoded

583 by *TPM1* and *TPM2* (right panel). (B) Coomassie gel showing the results of an A–Tpm3.1

584 cosedimentation assay. All samples contained 5 µM actin and increasing concentrations of

585 Tpm3.1 (1–15 µM) in a buffer containing 20 mM MOPS pH 7.3, 50 mM KCl, 5 mM $MgCl_2$.

586 (E) Binding curves showing the interaction of F–actin with Tpm1.6, Tpm1.12, Tpm2.1,

587 Tpm3.1, and Tpm4.2, in both the acetylated and non–acetylated forms. Fractional binding

588 (Tpm/actin) was determined using cosedimentation assays as depicted in panel B. The results

589 are shown normalized with 0 representing unbound and 1 fully bound Tpm isoforms. Data

590 were fitted using the Hill equation. Apparent binding affinities are summarized in Table 1. Four

591 independent experiments were carried out for each isoform, each with four individual

592 measurements. (D) Graph showing the temperature–induced dissociation (10 to 50°C) and

593 reassociation (50 to 10°C) of A–Tpm1.6 cofilaments, monitored by recording the associated

594 changes in light scattering intensity.

595

596 **Figure 3: Acetylation of Tpm results in isoform specific changes in the temperature–**

597 **induced dissociation of the cofilaments with F–actin as indicated by the decrease in light**

598 **scattering.** (A) N–terminal acetylation of Tpm1.6 at 10µM Tpm results in a shift of 1.6°C to

599 higher temperatures. (B) N–terminal acetylation of Tpm2.1 does not affect the dissociation

600 dynamics and T_{diss}. (C) N–terminal acetylation exerts a significantly higher impact on the T_{diss}

601 of the LMW Tpm isoforms. Acetylation of Tpm3.1 increases T_{diss} at 10µM by about 9°C (D)

602 N–terminal acetylation of Tpm4.2 leads to an even greater increase in T_{diss}, into a range where

603 denaturation of actin starts to interfere with the dissociation associated light scattering signal.

604 (E, F) Secondary plots showing the dependence of T_{diss} on [Tpm1.6] and [Tpm3.1] in the

605 absence and presence of N–terminal acetylation. Three independent experiments for each data

606 point were performed with each isoform. Symbols represent mean values ± S.D.

607

608 **Figure 4: Tpm–dependent changes in the kinetic and functional behavior of Myo1C^0–**

609 **ΔTH1.** (A) Cumming estimation plot showing the results of ATPase assays performed with

610 0.1 µM phosphorylated Myo–1C in the presence of filamentous β–actin (10 µM) or A–Tpm

611 cofilaments (10 µM). ATPase assays were performed at 37°C and results are given as ATP

612 turnover per myosin motor. At least three independent experiments were performed for each

613 experimental condition. The upper part of the Cumming estimation plot shows the results of

614 individual measurements as a swarmplot with mean ± SD represented by a broken line right

615 next to the data points. The lower part shows effect sizes as bootstrapped 95% confidence

616 intervals (CI) with a separate, aligned axis. If the 95% CI contains the null value and the vertical

617 bar is crossing the horizontal line of null effect, the combined results are considered not

618 statistically different. (B) Dose response curves for the inhibition of the motile activity of Myo–

619 1C by different cytoskeletal Tpm isoforms. Half maximal inhibitory concentrations (IC$_{50}$)

620 correspond to Tpm1.7 (1.0 ± 0.1 µM), Tpm1.6 (1.2 ± 0.2 µM), Tpm3.1 (1.3 ± 0.9 µM),

621 Tpm2.1 (4.2 ± 0.4 µM), and Tpm4.2 (1.5 ± 0.1 µM). Tpm1.12 (19.3 ± 1.1 µM). Sliding

19

622 velocities were measured at 37°C. (C) Tpm isoform–specific differences in the load–
623 dependence of Myo1C–driven movement of A–Tpm cofilaments were examined using the
624 frictional load assay (Greenberg and Moore, 2010). External loads applied by the addition of
625 increasing concentrations of α–actinin reduce the filament sliding velocity of bare F–actin and
626 cofilaments containing Tpm1.7 or Tpm3.1 to different extents. (D) The observed load–
627 dependent changes in sliding velocities are best described by a tension–sensing mechanism
628 that includes a force–dependent and a force–independent transition. (B–D) Values from at least
629 three independent experiments are shown as mean and SD. (Greenberg et al., 2015, 2012).

630 **Figure 5: Tpm–dependent changes in the kinetic and functional behavior of NM–2A.** (A)
631 Cumming estimation plot showing the results of ATPase assays performed with 0.5 μM
632 phosphorylated NM–2A–HMM in the presence of filamentous β–actin (20 µM) or A–Tpm
633 cofilaments (20 µM). Six or more independent experiments, each involving at least three
634 individual measurements, were performed for each experimental condition. (B) Cumming
635 estimation plot showing the results of *in vitro* motility assays performed with F–actin or A–
636 Tpm cofilaments on surfaces decorated with phosphorylated NM–2A–HMM. Seven or more
637 independent experiments, each involving at least five technical replicates with >100
638 trajectories, were performed for each experimental condition. All assays were performed at
639 30°C. For description of Cumming estimation plots see Figure 4 and quantification and
640 statistical analysis section.

641

642 **Figure 6: Tpm–dependent changes in actin–activated ATP turnover and functional**
643 **behavior of myosin–5A**. (A) Cumming estimation plot showing the results of ATPase assays
644 performed with 0.1 μM myosin–5A–HMM in the presence of filamentous β–actin (20 µM) or
645 A–Tpm cofilaments (20 µM). At least six independent experiments, each involving at least
646 four technical repeats, were performed for each experimental condition. (B) Cumming
647 estimation plot showing the results of *in vitro* motility assays performed with F–actin or A–
648 Tpm cofilaments on surfaces decorated with myosin–5A–HMM. Five or more independent
649 experiments, each involving at least four technical replicates with >100 trajectories, were
650 performed for each experimental condition. All assays were performed at 30°C. For description
651 of Cumming estimation plots see Figure 4 and quantification and statistical analysis section.

652

653 **Figure 7: N–terminal acetylation of Tpm–dependent changes in the kinetic and functional**

654 **behavior of NM–2A.** (A–D) The actin–activated ATPase activity of NM–2A–HMM was

655 measured with increasing [A–Tpm]. The assays were performed with 0.5 µM phosphorylated

656 NM–2A–HMM at 30°C. Six or more independent experiments, each involving at least three

657 individual measurements, were performed with each isoform. (E) Cumming estimation plot

658 showing the influence of the different Tpm isoforms and their acetylated form on the sliding

659 velocity of NM–2A. Seven or more independent experiments, each involving at least five

660 technical replicates with >100 trajectories, were performed with each isoform. For description

661 of Cumming estimation plots see Figure 4 and quantification and statistical analysis section.

662

663 **Figure 8: Changes in actin–activated ATP turnover and functional behavior of myosin–**

664 **5A mediated by N–terminal acetylation of Tpm**. (A) Cumming estimation plot showing the

665 results of ATPase assays performed with 0.1 µM myosin–5A–HMM in the presence of

666 filamentous β–actin ((20 µM) or A–Tpm cofilaments (20 µM). Two or more independent

667 experiments, each involving at least four technical repeats, were performed for each

668 experimental condition. (B) Cumming estimation plot showing the results of *in vitro* motility

669 assays performed with F–actin or A–Tpm cofilaments on surfaced decorated with myosin–5A–

670 HMM. Five or more independent experiments, each involving at least five technical replicates

671 with >100 trajectories, were performed for each experimental condition. All assays were

672 performed at 30°C. For description of Cumming estimation plots see Figure 4 and

673 quantification and statistical analysis section.

674

675 **TABLES**

676

677 **Table 1:** Apparent Tpm binding affinities ($K_{50\%}$) and temperature stability of A–Tpm

678 cofilaments

Tpm Isoform	Exon usage MW	$K_{50\%}$ [µM][§]	T_{diss} [°C][#]	T_{ass} [°C][#]	ΔT [°C]
Tpm1.6	1a.2b.6b.9d 32.7 kDa	1.32 ± 0.12	41.2 ± 0.6	39.0 ± 0.4	2.2 ± 0.6
AcTpm1.6	1a.2b.6b.9d 32.7 kDa	1.23 ± 0.14	39.6 ± 0.5	39.3 ± 0.4	0.3 ± 0.5
Tpm1.8	1b.–.6b.9d 28.6 kDa	0.1 ± 0.03	41.6 ± 0.1	39.0 ± 0.2	2.6 ± 0.2
Tpm1.12	1b.–.6b.9c 28.5 kDa	18.2 ± 1.5	n.d.	n.d.	n.d.
AcTpm1.12	1b.–.6b.9c 28.5 kDa	28.8 ± 1.9	47.5 ± 0.1[Ω]	n.d.	n.d.
Tpm2.1	1a.2b.6a.9d 32.9 kDa	1.73 ± 0.19	38.0 ± 0.1	37.4 ± 0.2	0.6 ± 0.2
AcTpm2.1	1a.2b.6a.9d 32.9 kDa	2.29 ± 0.23	37.6 ± 0.2	37.2 ± 0.3	0.4 ± 0.3
Tpm3.1	1b.–.6a.9d 29.0 kDa	1.50 ± 0.19	35.6 ± 0.4	29.8 ± 0.1	5.8 ± 0.4
AcTpm3.1	1b.–.6a.9d 29.0 kDa	1.15 ± 0.15	44.7 ± 0.7	43.6 ± 0.4	1.1 ± 0.7
Tpm4.2	1b.–.6b.9d 28.5 KDa	1.99 ± 0.83	36.5 ± 0.5	31.2 ± 0.3	5.3 ± 0.5
AcTpm4.2	1b.–.6b.9d 28.5 KDa	1.33 ± 0.41	> 50	n.d.	n.d.

679 [§] Experiments were performed in cosedimentation buffer containing 20 mM MOPS pH 7.0, 100 mM

680 KCl and 5 mM $MgCl_2$. The β–actin concentration was set to 5 µM, Tpm was titrated from 0.125 to 20

681 µM for all constructs with the exception of Tpm1.12, where the titration was performed over the range

682 0.125 to 40 µM. $K_{50\%}$ values were calculated after fitting the sigmoidal binding curves using the Hill

683 equation. At least four independent experiments were performed with each Tpm isoform.

684 [#] Experiments were performed in light–scattering buffer containing 20 mM potassium phosphate pH

685 7.4 and 50 mM NaCl. The β–actin concentration was set to 5 µM and the Tpm concentration to 10 µM.

686 T_{diss} and T_{ass} are the temperatures at which a 50% change in the intensity of the light scattering signal

687 occurs. At least three independent experiments, each involving 3 to 5 individual measurements, were

688 performed with each isoform. The results correspond to the mean value ± SD.

689 [Ω] Value taken from Marchenko et al., 2021 (Marchenko et al., 2021) for a recombinant Tpm1.12 with

690 an Ala–Ser N–terminal extension to mimic N–terminal acetylation. Experimental conditions: 10 µM

691 phalloidin–stabilized α–actin and 120 µM Ala–Ser–Tpm1.12 in 30 mM Hepes, 100 mM NaCl, 2 mM

692 DTT, pH7.3.

693 **Table 2:** Impact of changes in Tpm isoform on ATP turnover and unloaded velocity.

A–Tpm	Sliding velocity (nm s^{-1})	ATP turnover (s^{-1})	K$_{app}$ (µM)	k$_{cat}$/K$_{app}$ (µM^{-1}s^{-1})
	Myo1C^0–ΔTH1			
	(measured at 37°C)			
No Tpm	52.1 ± 4.9	0.17 ± 0.02$^\psi$ 0.38 ± 0.02§	12.42 ± 0.75	0.024 ± 0.001
Tpm1.6	11.5 ± 2.1	0.11 ± 0.03$^\psi$	n.d.	n.d.
Tpm1.7	10.5 ± 4.9	0.12 ± 0.02$^\psi$ 0.24 ± 0.02§	11.03 ± 0.60	0.015 ± 0.001
Tpm3.1	11.5 ± 1.7	0.11 ± 0.02$^\psi$ 0.25 ± 0.02§	12.03 ± 0.85	0.016 ± 0.001
Tpm2.1	11.8 ± 2.3	0.13 ± 0.02$^\psi$	n.d.	n.d.
Tpm4.2	10.4 ± 2.1	0.11 ± 0.03$^\psi$	n.d.	n.d.
	NM–2A–HMM			
	(measured at 30°C)			
No Tpm	103.2 ± 8.9	0.26 ± 0.02§	27.6 ± 6.7	0.0081 ± 0.0010
Tpm1.6	116.9 ± 19.5	0.35 ± 0.02§	27.8 ± 4.6	0.0124 ± 0.0015
AcTpm1.6	157.9 ± 21.3	0.31 ± 0.01§	17.7 ± 2.3	0.0174 ± 0.0015
Tpm2.1	115.9 ± 8.6	0.40 ± 0.04§	37.8 ± 11.1	0.0102 ± 0.0015
AcTpm2.1	124.6 ± 13.8	0.41 ± 0.03§	40.9 ± 7.3	0.0099 ± 0.0010
Tpm3.1	168.6 ± 15.2	0.64 ± 0.07§	19.6 ± 6.3	0.0291 ± 0.0020
AcTpm3.1	166.9 ± 10.1	0.48 ± 0.04§	26.6 ± 5.5	0.0180 ± 0.0010
Tpm4.2	98.5 ± 11.6	0.37 ± 0.02§	26.2 ± 5.6	0.0112 ± 0.0010
AcTpm4.2	145.7 ± 20.1	0.61 ± 0.06§	26.1 ± 6.1	0.0234 ± 0.0015
	Myosin–5A–HMM			
	(measured at 30°C)			
No Tpm	376.8 ± 20.7	1.05 ± 0.14$^\psi$	n.d.	n.d.
Tpm1.6	272.1 ± 36.2	0.71 ± 0.09$^\psi$	n.d.	n.d.
AcTpm1.6	262.9 ± 46.1	0.76 ± 0.10$^\psi$	n.d.	n.d.
Tpm1.12	423.0 ± 8.1	1.02 ± 0.08$^\#$	n.d.	n.d.
AcTpm1.12	397.9 ± 5.5	1.00 ± 0.11$^\#$	n.d.	n.d.
Tpm2.1	247.2 ± 22.5	0.64 ± 0.14$^\psi$	n.d.	n.d.
AcTpm2.1	277.2 ± 20.9	0.60 ± 0.06$^\psi$	n.d.	n.d.
Tpm3.1	256.7 ± 29.0	0.76 ± 0.07$^\psi$	n.d.	n.d.
AcTpm3.1	245.8 ± 29.0	0.74 ± 0.06$^\psi$	n.d.	n.d.
Tpm4.2	259.4 ± 18.1	0.61 ± 0.10$^\psi$	n.d.	n.d.
AcTpm4.2	247.1 ± 7.3	0.61 ± 0.13$^\psi$	n.d.	n.d.

§ **The actin–activated ATPase activities of NM–2A–HMM and Myo1C^0–ΔTH1 were measured as a function of [A] or [A–Tpm]. Values for k$_{cat}$ and K$_{app}$ were calculated by fitting the data to the Michaelis–Menten equation. R^2 was within the range of 0.92 to 0.99. At least six independent ATPase assays were performed, each involving 3 to 5 individual measurements.**

$^{\Psi}$ **Actin–activated ATPase activity measured in the presence of 20 µM F–actin and 15 µM Tpm, except the low affinity Tpm1.12, where 30 µM were used. Control measurements were performed with 20 µM F–actin in the absence of Tpm. At least four independent experiments were performed, each involving 3 to 5 individual measurements. Results correspond to the mean value ± SD.**

$^{\#}$ **Actin–activated ATPase activity measured in the presence of 20 µM F–actin and 30 µM Tpm. Control measurements were performed with 20 µM F–actin in the absence of Tpm. At least four independent experiments were performed, each involving 3 to 5 individual measurements. Results correspond to the mean value ± SD.**

694

695 **Table 3:** Impact of changes in Tpm isoform on the transient kinetic parameters for acto–
696 Myo1C[0]

	Signal and measured parameter	No Tpm	Tpm1.7	Tpm3.1
Active site isomerization				
K_α	Pyrene–actin; A_{fast}/A_{slow}	0.90 ± 0.03	0.76 ± 0.06	0.73 ± 0.06
$k_{+\alpha}$ (s^{-1}) (20°C)	Pyrene–actin, $k_{max,slow}$	4.1 ± 0.2	3.2 ± 0.2	3.2 ± 0.2
(37°C)		9.7 ± 0.4	10.7 ± 0.8	9.9 ± 0.3
$k_{-\alpha}$ (s^{-1})	$k_{+\alpha} / K_\alpha$ (calc.)	4.56 ± 0.37	4.21 ± 0.46	4.38 ± 0.63
ATP-binding to actomyosin				
$1/K_1$ (µM)				
k_{+2} (s^{-1}) (20°C)	Pyrene–actin, $K_{0.5,fast}$	154 ± 31	136 ± 14	134 ± 19
(37°C)	Pyrene–actin, $k_{max,fast}$	37.1 ± 1.6	23.0 ± 0.5	22.3 ± 0.7
K_1k_{+2} (µM^{-1} s^{-1}) [a]		69.5 ± 1.9	70.1 ± 1.8	76.8 ± 1.7
	Pyrene–actin, initial slope	0.16 ± 0.01	0.12 ± 0.01	0.12 ± 0.01
Actomyosin binding				
(in absence of nucleotides)				
k_{+A} (µM^{-1} s^{-1}) [b]	Pyrene–actin, slope	1.46 ± 0.07	1.33 ± 0.03	1.36 ± 0.04
k_{-A} (s^{-1})	Pyrene–actin, k_{obs}	0.019 ± 0.001	0.025 ± 0.001	0.025 ± 0.001
K_A (nM)	k_{-A} / k_{+A} (calc.)	13.7 ± 0.1	19.6 ± 0.2	18.4 ± 0.3
Phosphate release				
k_{obs} (s^{-1}) [c]	MDCC–PBP	0.021 ± 0.001	0.015 ± 0.001	0.015 ± 0.001
k_{+4} (s^{-1})	(calc.)	0.09 ± 0.01	0.07 ± 0.01	0.05 ± 0.01
ADP binding of actomyosin				
K_5 (µM) [d]	Pyrene–actin, A_{slow}/A_{total}	0.46 ± 0.08	0.32 ± 0.17	0.29 ± 0.15
k_{+5} (s^{-1}) (20°C)	Pyrene–actin, $k_{min,slow}$	1.59 ± 0.07	1.11 ± 0.09	1.05 ± 0.05
(37°C)		7.8 ± 0.1	7.3 ± 0.3	7.1 ± 0.2
k_{-5} (µM^{-1} s^{-1})	k_{+5} / K_5 (calc.)	3.45 ± 0.75	3.47 ± 2.12	3.62 ± 2.05

25 mM HEPES pH 7.5, 50 mM KCl, 5 mM MgCl$_2$, 0.5 mM DTT at 20°C, unless otherwise specified; [a] derived from the initial slope of the plot $k_{obs,fast}$ versus [ATP]; [b] derived from the slope of the plot k_{obs} versus [actin]; [c] in the presence of 5 µM F–actin at 20°C, values for k_{+4} in the presence of saturating [actin] and at 20°C are estimated on the basis of the steady–state ATPase measurements; [d] derived from the fit A_{slow}/A_{total} = [ADP] / (K_5 + [ADP]).

697
698

699

700 **STAR★METHODS**

701 **RESOURCE AVAILABILITY**

702

703 **Lead contact**

704 Further information and requests for resources and reagents should be directed to, and will be

705 fulfilled by the corresponding author and Lead Contact, Dietmar J. Manstein

706 (Manstein.Dietmar@MH-Hannover.de).

707

708 **Materials availability**

709 All unique/stable reagents generated in this study are available from the Lead Contact with a

710 completed Materials Transfer Agreement.

711

712 **Data and code availability**

713 The published article includes all data generated or analyzed during this study. Any additional

714 information required to reanalyze the data reported in this paper is available from the lead

715 contact upon request. This paper does not report original code.

716

717 **EXPERIMENTAL MODEL AND SUBJECT DETAILS**

718 Sf9 *(Spodoptera frugiperda)* cells adapted to Sf-900™ II SFM were purchased from Thermo

719 Fisher/Gibco (Cat#11496015) and used for the production of recombinant proteins according

720 to the manufacturer's instructions and as described in the methods section.

721

722 **METHOD DETAILS**

723 *Reagents*

724 All chemicals and reagents were of the highest purity commercially available. ATP, *N*–(1–

725 Pyrene)iodoacetamide), EGTA, HEPES, MOPS were purchased from (Merck KGaA,

726 Darmstadt, Germany).

727 *Constructs and proteins*

728 Human Myo1C^0–ΔTH1 (UniProtKB - O00159–2; residues 1–856) was co–produced with CaM

729 from pFastBac^{TM} dual vector and purified from *Sf9* cells using Immobilized Metal Affinity

730 Chromatography (IMAC; Ni-NTA) and size exclusion chromatography (SEC; Superdex 200

731 10/300 column) as described earlier (Münnich et al., 2014). Additionally, human CaM was

26

732 produced in *E. coli* Rosetta pLySs (DE3) using a pET–3a vector. The over–produced tag–free

733 CaM was purified using an initial heat precipitation step. The cell lysate was incubated at 70°C

734 in a water bath for 10 min to remove most contaminating proteins by denaturation and

735 aggregation, while CaM remains stable and soluble. Following centrifugation for 30 min at

736 100,000 *g*, the supernatant was loaded onto a phenyl sepharose column, washed with 50 mM

737 HEPES pH 7.5, 200 mM NaCl, 5 mM DTT, 4 mM MgCl$_2$, 1 mM EGTA and pure CaM was

738 eluted with 50 mM HEPES pH7.5, 1 mM EGTA (Münnich and Manstein, 2013).

739 The HMM fragment of human NM–2A (UniProtKB - P35579) with C–terminal His8– and

740 Avi–tags was overproduced in complex with non–muscle essential light chain (MYL6;

741 UniProtKB - P60660) and regulatory light chain (MYL12b; UniProtKB - O14950) using the

742 baculovirus/Sf9 system. Cells were harvested, lysed (50 mM HEPES pH 7.5, 200 mM NaCl,

743 15 mM MgCl2, 4 mM ATP, 0.3 mM EGTA, 0.3 mM EDTA, 5% Glycerol, 1mM DTT and

744 protease inhibitor cocktail) by sonication and purified by IMAC and SEC (Superdex 200

745 10/300; 25mM Hepes pH 7.3, 200mM NaCl, 1mM EDTA, 1mM EGTA, 1mM DTT). NM–

746 2A–HMM was phosphorylated immediately prior to use at 30°C for 30 min. NM–2A–HMM

747 was incubated with myosin light chain kinase at a stoichiometric ratio of 20:1 in a reaction

748 mixture containing 20 mM MOPS pH 7.0, 50 mM KCl, 2 mM MgCl$_2$, 1 mM CaCl$_2$, 0.15 mM

749 EGTA, 0.2 µM calmodulin, 2 mM DTT and 2 µM of each, ELC and RLC.

750 The HMM fragment (residues 1–1098, Cloning-Primer listed in Table S1) of human myosin–

751 5A (UniProtKB - Q9Y4I1) with C–terminal His8– and Avi–tags was overproduced using the

752 baculovirus/Sf9 system and purified in complex with calmodulin–1 (CaM) (UniProtKB -

753 P0DP23) according to the protocol used for NM–2A HMM. The residues forming the HMM

754 fragment of human myosin–5A are identical for the three isoforms produced by alternative

755 splicing.

756 The human β–actin (UniProtKB P60709) and γ–actin (UniProtKB - P63261) isoforms were

757 overproduced and purified using the baculovirus/Sf9 system as described for mouse β–actin

758 (Noguchi et al., 2007). In brief, cells were lysed (20 mM Tris pH8, 50mM KCl, 5Mm CaCl$_2$,

759 4% Triton X-100, 1 mg/ml Tween 20, 1mM ATP, 10mM Imidazole, 1mM DTT) by sonication

760 and incubated with His-tagged gelsolin (G4-6) overnight. The soluble fraction was incubated

761 with Ni-NTA and actin was eluted via a chelator of Ca^{2+}, EGTA. Actin containing fractions

762 were polymerized with 150 mM KCl and F-actin separated by centrifugation. F-actin

763 resuspended and dialyzed (10mM Tris pH8, 1mM CaCl$_2$, 50mM KCl, 1mM DTT) overnight.

764 The polymerization-depolymerization procedure was repeated. Chicken skeletal muscle α–

765　actin (UniProtKB - P68139) was purified according to the method of Lehrer and Kerwar with

766　slight modifications (Diensthuber et al., 2011; Lehrer and Kerwar, 1972). Human Tpm1.6

767　(NCBI Reference Sequence NP_001018004.1), Tpm1.8 (NCBI Reference Sequence

768　NP_001288218.1), Tpm1.12 (NCBI Reference Sequence NP_001018008.1), Tpm2.1 (NCBI

769　Reference Sequence NP_998839.1), Tpm3.1 (NCBI Reference Sequence NP_705935.1) and

770　Tpm4.2 (NCBI Reference Sequence NP_003281.1) were produced tag–free in *E. coli.* The

771　amino terminal–acetylated Tpm isoforms were produced using coexpression of Tpm1.12,

772　Tpm3.1 or Tpm4.2 with the fission yeast NatA complex (Naa10, UniProtKB - Q9UTI3; Naa15,

773　UniProtKB - O74985). Tpm1.6 and Tpm2.1 were coproduced in *E. coli* with the NatB complex

774　(Naa20, UniProtKB - O74457; Naa25, UniProtKB - Q9Y809) (Eastwood et al., 2017).

775　Oligonucleotide sequences used for cloning are listed in Table S1. *E. coli* lysates (50mM Hepes

776　pH7.5, 200 mM NaCl, 5mM MgCl$_2$, 5mM DTT, 0.5 mg/ml lysozyme, protease inhibitor) after

777　overproducing acetylated and non–acetylated Tpm1.6, Tpm2.1, Tpm3.1 and Tpm4.2 was

778　heated up to 80°C for 10 minutes and cooled on ice. The soluble fraction was filtered and Tpm

779　precipitated at the respective pI. The precipitate was separated by centrifugation and

780　resuspended in low salt buffer (20mM Tris pH7.2, 100mM NaCl, 5mM MgCl$_2$) for anion

781　exchange chromatography. Tpm containing fractions were concentrated by precipitation. All

782　vectors used for protein production were confirmed by sequencing. Protein concentration was

783　determined using the Bradford assay and by recording protein absorbance spectra of the region

784　from 240 to 400 nm with a UV–2600 spectrophotometer (Shimadzu Deutschland GmbH,

785　Duisburg, Germany). Molar extinction coefficients at 280 nm were calculated from the amino

786　acid composition (Gill and von Hippel, 1989).

787　***Antibodies***

788　Antibodies used in this study include the mouse monoclonal antibody QIAexpress Penta·His,

789　BSA–free (Qiagen, catalogue no. 34650); the Tpm–specific sheep polyclonal antibodies

790　TPM3/9d (Merck Millipore, catalogue no. AB5447), TPM1/1b (Merck Millipore, catalogue

791　no. ABC499), and TPM1/9d (Merck Millipore, catalogue no. AB5441); donkey anti–sheep

792　IgG–HRP secondary antibody (Santa Cruz Biotechnology, catalogue no. sc–2473). Rabbit

793　polyclonal antibody D55Ac was raised against the peptide Ac–MDAIKKKMQMLKLD

794　(Eurogentec, Seraing, Belgium). D55Ac specifically detects N–acetylated isoforms derived

795　from *TPM1* and *TPM2* that share the use of exon 1a. The epitope is found in Tpm1.1, Tpm1.2,

796　Tpm1.3, Tpm1.4, Tpm1.5, Tpm1.6, Tpm1.7, Tpm1.10, Tpm2.1, Tpm2.2, Tpm2.3, and

797　Tpm2.4.

Cosedimentation assays

Affinities of the different Tpm isoforms for filamentous β–actin were analyzed by means of co–sedimentation assays. Varying Tpm concentrations (0 to 20 μM) were incubated with 5 μM filamentous β–actin for 30 min at 21°C in cosedimentation buffer (20 mM MOPS pH 7.0, 100 mM KCl and 5 mM MgCl$_2$). Ultracentrifugation was used to separate A–Tpm cofilaments from free Tpm (30 min, 100,000 g at 10°C). Supernatant and pellet fractions were subsequently resolved by sodium dodecyl sulphate–polyacrylamide gel electrophoresis. Protein bands were quantified by densitometry using a Bio–Rad ChemiDoc^{TM} MP system (Bio–Rad Laboratories, Inc., Hercules, CA, USA) and the Fiji release of ImageJ software version 1.49s (Schindelin et al., 2012). Four independent experiments were carried out for each acetylated and non–acetylated Tpm isoform, each with four individual measurements. The binding coefficients (K$_{50\%}$) were determined by fitting the sigmoidal binding curves with the Hill equation.

Light scattering assays

It has been shown that the temperature–induced dissociation of A–Tpm cofilaments can be followed by changes in the intensity of the light scattering signal at 350 nm (Wegner, 1979). A Cary Eclipse fluorescence spectrophotometer and the Thermal Application Module (Agilent Technologies, Santa Clara, CA, U.S.A.) were used to record the change in the light scattering signal as a function of temperature. Heating and cooling rates were set to 0.5°C/min. The buffers used for light scattering assays contained 20 mM potassium phosphate pH 7.4 and 50 mM NaCl 5 μM actin and 10 μM Tpm. Control measurements performed at different Tpm concentrations in the absence of actin did not result in a change of the light scattering signal. After complete dissociation of Tpm from A–Tpm cofilaments, the light scattering signal equals the signal of bare F–actin. Assuming that A–Tpm cofilament dissociation and association correspond to a two–state process, the observed sigmoidal temperature dependences can be fitted with a Boltzmann function. The inflection points of the sigmoidal curves define the respective transition temperature T$_{diss}$ and T$_{ass}$ for the different Tpm isoforms.

Kinetic measurements

The regulatory light chain of NM–2A–HMM was phosphorylated for 30 min at 30 °C in kinase buffer (20 mM MOPS pH 7.0, 50 mM KCl, 2 mM MgCl$_2$, 0.15 mM EGTA, 2 mM DTT) containing 1 mM CaCl$_2$, 0.2 μM CaM, 2 μM essential light chain (MYL6), 2 μM regulatory light chain (MYL12b), 1 mM ATP and 50 nM myosin light chain kinase. The steady–state ATPase rates of NM–2A and myosin–5A were measured using an NADH–coupled assay (Furch et al., 1998) in ATPase buffer–I containing 0.5 μM NM–2A–HMM or 0.1 μM myosin–

29

831   5A, 20 mM MOPS pH 7.3, 50 mM KCl, 5 mM MgCl$_2$, 1 mM ATP, 0.8 mM NADH, 0.5 mM

832   phosphoenolpyruvate, 20 µg/ml lactate dehydrogenase, 50 µg/ml pyruvate kinase at 30°C.

833   Steady–state ATP turnover by myosin–1C^0 was measured in ATPase buffer–II containing

834   0.1 µM Myo1C^0–ΔTH1, 25 mM HEPES pH 7.5, 50 mM KCl, 5 mM MgCl$_2$, 0.5 mM DTT,

835   1 mM ATP, 0.4 mM NADH, 0.5 mM phosphoenolpyruvate, 20 µg/ml lactate dehydrogenase

836   and 50 µg/ml pyruvate kinase at 37°C. [A] or [A–Tpm] was varied over the range from 0 to 50

837   µM. The change in absorption at 340 nm was recorded in 96–well plates on a CLARIOstar Plus

838   microplate reader (BMG Labtech, Ortenberg, Germany) (Giese et al., 2020). All combinations

839   were tested with and without the addition of myosin, and the actin ATPase rate was then

840   subtracted from the myosin ATPase rates. For titrations, increasing concentrations of

841   filamentous actin were pre–incubated with the different Tpm isoforms for 30 min at room

842   temperature, before addition to the assay mix. To ensure that Tpm is present in saturating

843   concentration, 20 µM Tpm was added in all experiments. The parameters k_{cat}, $K_{app.actin}$, and

844    $k_{cat}/K_{app.actin}$ were obtained by fitting the data to the Michaelis–Menten equation. $K_{app.actin}$ is the

845   apparent dissociation equilibrium constant for actin or actin–Tpm binding in the presence of

846   ATP, k_{cat} gives the maximum value of the ATPase activity, and $k_{cat}/K_{app.actin}$ corresponds to the

847   apparent second order rate constant for actin binding, which indicates the coupling efficiency

848   between actin and nucleotide binding. At concentrations of actin much lower than $K_{app.actin}$,

849    $k_{cat}/K_{app.actin}$ is well–defined by the slope of the initial linear part of the dependence. Estimation

850   statistics are depicted as a Cumming estimation plot (Cumming, 2011; Ho, Tumkaya, Aryal,

851   Choi, & Claridge–Chang, 2019). At least four independent ATPase assays were performed

852   with myosin–5A and at least six with NM–2A–HMM and Myo1C^0–ΔTH1. Three to five

853   technical replicates were performed during each assay.

854   Transient kinetic experiments were performed at 20°C in a buffer containing 25 mM HEPES,

855   pH 7.5, 5 mM MgCl$_2$, 0.5 mM DTT, and 50 mM KCl using either a HiTech Scientific SF–

856   61 DX or a HiTech SF–61 SX stopped–flow system (TgK Scientific Ltd, Bradford–on–Avon,

857   U.K.) (Heissler & Manstein, 2012; Hundt et al., 2016; Pathan–Chhatbar et al., 2018). Kinetic

858   parameters for the interaction of myosin motor domains with nucleotide and F–actin were

859   analyzed in terms of the kinetic model shown for Myo1C^0–ΔTH1 in Figure 1C (Giese et al.,

860   2020). Rate constants are referred to as k$_{+n}$ and k$_{-n}$, respectively. Dissociation equilibrium

861   constants are denoted as K$_n$. K$_A$ represents the affinity of myosin for F–actin in the absence of

862   nucleotide. The equilibrium constant K$_\alpha$ for the closed–to–open isomerization of the nucleotide

863   binding pocket and the isomerization rate $k_{+\alpha}$ were determined by monitoring the fluorescence

864   change during the ATP-induced dissociation of pyrene-labeled acto–Myo1C–ΔTH1 (130 nM)

865   following mixing with 0.03 to 10 mM ATP. The observed fluorescence transients are best

866   described by double exponentials. The data for the ratio of slow to fast phase amplitudes

867   (A_{slow}/A_{fast}) plotted against the ATP concentration are best–fitted to a hyperbola, where the

868   plateau value defines K_α. The dependence of $k_{obs,slow}$ on ATP concentration are best–fitted with

869   a hyperbola, where the plateau values define $k_{+\alpha}$ (Giese et al., 2020). Kinetic Studio software

870   (TgK Scientific Ltd., Bradford on Avon, UK) was used for initial data inspection and analysis

871   of transient kinetic data. Detailed data analysis was performed with Origin Pro 9.55 (OriginLab

872   Corporation, Northampton, MA, USA) graphing and data analysis software. Each data point

873   corresponds to the average of 3 to 5 single measurements. Goodness–of–fit criteria were

874   evaluated using the coefficient of determination R^2 and χ^2 tests as implemented in Origin Pro

875   9.55.

876   ***Myosin motor activity assays***

877   Unloaded *in vitro* motility assays were performed as described (Kron and Spudich, 1986) with

878   the following modifications. F–actin was labelled with phalloidin–tetramethyl rhodamine B

879   isothiocyanate (Merck KGaA, Darmstadt, Germany) overnight at 4°C. To determine the

880   appropriate conditions for fast and constant velocities, we performed initial titrations of motor

881   activity with each myosin construct in the presence of labelled F–actin. We determined 0.2

882   mg/ml Myo1C^0–ΔTH1, 0.2 mg/ml NM–2A and 0.01 mg/ml myosin–5A as optimal

883   concentrations. Where appropriate, actin was pre–incubated with 15 μM Tpm. In these cases,

884   Tpm was added to all buffer solutions used. For His–tagged Myo1C^0–ΔTH1, one chamber

885   volume (10 μl) of 0.05 mg/ml His antibody (QIAexpress® mouse monoclonal Penta·His™)

886   was infused into the flow chamber and incubated for 5 min. Free positions on the surface were

887   blocked with 0.5 mg/ml BSA in assay buffer (20 mM MOPS pH 7.3, 50 mM KCl, 5 mM

888   MgCl$_2$). Actin sliding motility was measured at 30°C (NM–2A and myosin–5A) or 37°C

889   (Myo1C^0–ΔTH1) using an Olympus IX70 or IX81 fluorescence microscope equipped with a

890   60×/1.49 NA PlanApo objective and an Orca Flash 4.0 CMOS camera (Hamamatsu Photonics,

891   Herrsching, Germany). Independent *in vitro* motility assays were performed with two flow

892   cells per isoform, where three or more video sequences of 180 sec were recorded and at least

893   400 filaments were tracked per sequence. Sliding velocities were determined using the ImageJ

894   plugin *wrMTrck* (Schindelin et al., 2012) and Origin V9.55 (OriginLab Corporation,

895   Northampton, MA, USA). Estimation statistics are depicted as a Cumming estimation plot

896   (Cumming, 2011; Ho et al., 2019). Frictional loading assays were performed in the presence

897   of rising concentrations of α–actinin to generate increasing viscoelastic loads on the actin

898 filaments and at a surface density of 3,600 Myo1C^0–ΔTH1 motors µm^{-2} (Greenberg and

899 Moore, 2010). Results were analyzed according to (Ngo et al., 2016).

900 *Quantification and statistical analysis*

901 Estimation statistics for the results of kinetic and *in vitro* motility measurements were obtained

902 using the DABEST plugin for Python (Ho et al., 2019) and depicted as a Cumming estimation

903 plot, a variation of the Gardner– Altman Multi–group estimation plot (Cumming, 2011; Ho et

904 al., 2019). Estimation statistics focuses on effect size measuring the strength of the relationship

905 between two variables on a numeric scale. The results of the individual measurements are

906 shown as a swarmplot with mean ± standard deviation (SD) represented by a broken line. Effect

907 sizes are shown as bootstrapped 95% confidence intervals (CI) on a separate, aligned axis. If

908 the 95% CI contains the null value and the vertical bar is crossing the horizontal line of null

909 effect, the combined results are considered not statistically different.

910

911 **REFERENCES**

912 Adamek, N., Coluccio, L.M., Geeves, M.A., 2008. Calcium sensitivity of the cross-bridge
913   cycle of Myo1c, the adaptation motor in the inner ear. Proc. Natl. Acad. Sci. U. S. A. 105,
914   5710–5. https://doi.org/10.1073/pnas.0710520105

915 Arnesen, T., Van Damme, P., Polevoda, B., Helsens, K., Evjenth, R., Colaert, N., Varhaug,
916   J.E., Vandekerckhove, J., Lillehaug, J.R., Sherman, F., Gevaert, K., 2009. Proteomics
917   analyses reveal the evolutionary conservation and divergence of N-terminal
918   acetyltransferases from yeast and humans. Proc. Natl. Acad. Sci. 106, 8157–8162.
919   https://doi.org/10.1073/pnas.0901931106

920 Bareja, I., Wioland, H., Janco, M., Nicovich, P.R., Jégou, A., Romet-Lemonne, G., Walsh, J.,
921   Böcking, T., 2020. Dynamics of Tpm1.8 domains on actin filaments with single-molecule
922   resolution. Mol. Biol. Cell 31, 2452–2462. https://doi.org/10.1091/mbc.E19-10-0586

923 Barua, B., Nagy, A., Sellers, J.R., Hitchcock-DeGregori, S.E., 2014. Regulation of nonmuscle
924   myosin II by tropomyosin. Biochemistry 53, 4015–24. https://doi.org/10.1021/bi500162z

925 Barua, B., Sckolnick, M., White, H.D., Trybus, K.M., Hitchcock-DeGregori, S.E., 2018.
926   Distinct sites in tropomyosin specify shared and isoform-specific regulation of myosins
927   II and V. Cytoskeleton 75, 150–163. https://doi.org/10.1002/cm.21440

928 Boguslavsky, S., Chiu, T., Foley, K.P., Osorio-Fuentealba, C., Antonescu, C.N., Bayer, K.U.,
929   Bilan, P.J., Klip, A., 2012. Myo1c binding to submembrane actin mediates insulin-
930   induced tethering of GLUT4 vesicles. Mol. Biol. Cell 23, 4065–78.
931   https://doi.org/10.1091/mbc.E12-04-0263

932 Bonello, T.T., Janco, M., Hook, J., Byun, A., Appaduray, M., Dedova, I., Hitchcock-
933   DeGregori, S., Hardeman, E.C., Stehn, J.R., Böcking, T., Gunning, P.W., 2016. A small
934   molecule inhibitor of tropomyosin dissociates actin binding from tropomyosin-directed
935   regulation of actin dynamics. Sci. Rep. 6, 19816. https://doi.org/10.1038/srep19816

936 Brettle, M., Patel, S., Fath, T., 2016. Tropomyosins in the healthy and diseased nervous system.
937   Brain Res. Bull. 126, 311–323. https://doi.org/10.1016/j.brainresbull.2016.06.004

938 Bryce, N.S., Schevzov, G., Ferguson, V., Percival, J.M., Lin, J.J.-C., Matsumura, F., Bamburg,
939   J.R., Jeffrey, P.L., Hardeman, E.C., Gunning, P., Weinberger, R.P., 2003. Specification
940   of Actin Filament Function and Molecular Composition by Tropomyosin Isoforms. Mol.
941   Biol. Cell 14, 1002–1016. https://doi.org/10.1091/mbc.e02-04-0244

942 Carman, P.J., Barrie, K.R., Dominguez, R., 2021. Novel human cell expression method reveals
943   the role and prevalence of posttranslational modification in nonmuscle tropomyosins. J.
944   Biol. Chem. 297, 101154. https://doi.org/10.1016/j.jbc.2021.101154

945 Cho, Y.J., Hitchcock-DeGregori, S.E., 1991. Relationship between alternatively spliced exons
946   and functional domains in tropomyosin. Proc. Natl. Acad. Sci. U. S. A. 88, 10153–7.
947   https://doi.org/10.1073/pnas.88.22.10153

948 Christensen, J.R., Hocky, G.M., Homa, K.E., Morganthaler, A.N., Hitchcock-DeGregori, S.E.,
949   Voth, G.A., Kovar, D.R., 2017. Competition between Tropomyosin, Fimbrin, and
950   ADF/Cofilin drives their sorting to distinct actin filament networks. Elife 6.
951   https://doi.org/10.7554/eLife.23152

952 Clayton, J.E., Pollard, L.W., Murray, G.G., Lord, M., 2015. Myosin motor isoforms direct
953   specification of actomyosin function by tropomyosins. Cytoskeleton (Hoboken). 72, 131–
954   45. https://doi.org/10.1002/cm.21213

955 Clayton, J.E., Pollard, L.W., Sckolnick, M., Bookwalter, C.S., Hodges, A.R., Trybus, K.M.,
956   Lord, M., 2014. Fission yeast tropomyosin specifies directed transport of myosin-V along
957   actin cables. Mol. Biol. Cell 25, 66–75. https://doi.org/10.1091/mbc.E13-04-0200

958 Coulton, A., Lehrer, S.S., Geeves, M.A., 2006. Functional homodimers and heterodimers of
959   recombinant smooth muscle tropomyosin. Biochemistry 45, 12853–8.
960   https://doi.org/10.1021/bi0613224

961 Cumming, G., 2011. Understanding the new statistics : effect sizes, confidence intervals, and
962   meta-analysis. Routledge.

963 De La Cruz, E.M., Wells, A.L., Rosenfeld, S.S., Ostap, E.M., Sweeney, H.L., 1999. The kinetic
964   mechanism of myosin V. Proc. Natl. Acad. Sci. 96, 13726–13731.
965   https://doi.org/10.1073/pnas.96.24.13726

966 Diensthuber, R.P., Müller, M., Heissler, S.M., Taft, M.H., Chizhov, I., Manstein, D.J., 2011.
967   Phalloidin perturbs the interaction of human non-muscle myosin isoforms 2A and 2C1
968   with F-actin. FEBS Lett. 585, 767–71. https://doi.org/10.1016/j.febslet.2011.01.042

969 Dufour, C., Weinberger, R.P., Gunning, P., 1998. Tropomyosin isoform diversity and neuronal
970   morphogenesis. Immunol. Cell Biol. 76, 424–9. https://doi.org/10.1046/j.1440-
971   1711.1998.00765.x

972 East, D.A., Sousa, D., Martin, S.R., Edwards, T.A., Lehman, W., Mulvihill, D.P., 2011.
973   Altering the stability of the Cdc8 overlap region modulates the ability of this tropomyosin
974   to bind co-operatively to actin and regulate myosin. Biochem. J. 438, 265–73.
975   https://doi.org/10.1042/BJ20101316

976 Eastwood, T.A., Baker, K., Brooker, H.R., Frank, S., Mulvihill, D.P., 2017. An enhanced
977   recombinant amino-terminal acetylation system and novel in vivo high-throughput screen
978   for molecules affecting α-synuclein oligomerisation. FEBS Lett. 591, 833–841.
979   https://doi.org/10.1002/1873-3468.12597

980 Eaton, B.L., 1976. Tropomyosin binding to F-actin induced by myosin heads. Science 192,
981   1337–9. https://doi.org/10.1126/science.131972

982 Fischer, S., Rynkiewicz, M.J., Moore, J.R., Lehman, W., 2016. Tropomyosin diffusion over

983 actin subunits facilitates thin filament assembly. Struct. Dyn. (Melville, N.Y.) 3, 012002.
984 https://doi.org/10.1063/1.4940223

985 Furch, M., Geeves, M.A., Manstein, D.J., 1998. Modulation of actin affinity and actomyosin
986 adenosine triphosphatase by charge changes in the myosin motor domain. Biochemistry
987 37, 6317–6326. https://doi.org/10.1021/bi972851y

988 Gateva, G., Kremneva, E., Reindl, T., Kotila, T., Kogan, K., Gressin, L., Gunning, P.W.,
989 Manstein, D.J., Michelot, A., Lappalainen, P., 2017. Tropomyosin Isoforms Specify
990 Functionally Distinct Actin Filament Populations In Vitro. Curr. Biol. 27, 705–713.
991 https://doi.org/10.1016/j.cub.2017.01.018

992 Geeves, M. a., Hitchcock-DeGregori, S.E., Gunning, P.W., 2015. A systematic nomenclature
993 for mammalian tropomyosin isoforms. J. Muscle Res. Cell Motil. 36, 147–153.
994 https://doi.org/10.1007/s10974-014-9389-6

995 Geeves, M.A., 1989. Dynamic interaction between actin and myosin subfragment 1 in the
996 presence of ADP. Biochemistry 28, 5864–5871. https://doi.org/10.1021/bi00440a024

997 Giese, S., Reindl, T., Reinke, P.Y.A., Zattelman, L., Fedorov, R., Henn, A., Taft, M.H.,
998 Manstein, D.J., 2020. Mechanochemical properties of human myosin 1C are modulated
999 by isoform-specific differences in the N-terminal extension. J. Biol. Chem. 296.
1000 https://doi.org/10.1074/jbc.RA120.015187

1001 Gill, S.C., von Hippel, P.H., 1989. Calculation of protein extinction coefficients from amino
1002 acid sequence data. Anal. Biochem. 182, 319–26. https://doi.org/10.1016/0003-
1003 2697(89)90602-7

1004 Greaseri, M.L., Gergely, J., 1971. Reconstitution of Troponin Activity from Three Protein
1005 Components*, J. Biol. Chem. https://doi.org/10.1016/S0021-9258(18)62075-7

1006 Greenberg, M.J., Lin, T., Goldman, Y.E., Shuman, H., Ostap, E.M., 2012. Myosin IC generates
1007 power over a range of loads via a new tension-sensing mechanism. Proc. Natl. Acad. Sci.
1008 U. S. A. 109, E2433-40. https://doi.org/10.1073/pnas.1207811109

1009 Greenberg, M.J., Lin, T., Shuman, H., Ostap, E.M., 2015. Mechanochemical tuning of myosin-
1010 I by the N-terminal region. Proc. Natl. Acad. Sci. U. S. A. 112, E3337-44.
1011 https://doi.org/10.1073/pnas.1506633112

1012 Greenberg, M.J., Moore, J.R., 2010. The molecular basis of frictional loads in the in vitro
1013 motility assay with applications to the study of the loaded mechanochemistry of molecular
1014 motors. Cytoskeleton (Hoboken). 67, 273–85. https://doi.org/10.1002/cm.20441

1015 Greene, L.E., Eisenberg, E., 1980. Cooperative binding of myosin subfragment-1 to the actin-
1016 troponin-tropomyosin complex. Proc. Natl. Acad. Sci. U. S. A. 77, 2616–20.
1017 https://doi.org/10.1073/pnas.77.5.2616

1018 Greenfield, N.J., Stafford, W.F., Hitchcock-DeGregori, S.E., 1994. The effect of N-terminal
1019 acetylation on the structure of an N-terminal tropomyosin peptide and alpha alpha-
1020 tropomyosin. Protein Sci. 3, 402–10. https://doi.org/10.1002/pro.5560030304

1021 Gunning, P., O'neill, G., Hardeman, E., 2008. Tropomyosin-based regulation of the actin
1022 cytoskeleton in time and space. Physiol. Rev. 1–35.
1023 https://doi.org/10.1152/physrev.00001.2007.

1024 Gunning, P.W., Schevzov, G., Kee, A.J., Hardeman, E.C., 2005. Tropomyosin isoforms:
1025 divining rods for actin cytoskeleton function. Trends Cell Biol. 15, 333–41.
1026 https://doi.org/10.1016/j.tcb.2005.04.007

1027 Heald, R.W., Hitchcock-DeGregori, S.E., 1988. The structure of the amino terminus of

1028   tropomyosin is critical for binding to actin in the absence and presence of troponin. J.
1029   Biol. Chem. 263, 5254–9.

1030   Heissler, S.M., Manstein, D.J., 2012. Functional characterization of the human myosin-7a
1031   motor domain. Cell. Mol. Life Sci. 69, 299–311. https://doi.org/10.1007/s00018-011-
1032   0749-8

1033   Hendricks, M., Weintraub, H., 1981. Tropomyosin is decreased in transformed cells. Proc.
1034   Natl. Acad. Sci. 78, 5633–5637. https://doi.org/10.1073/pnas.78.9.5633

1035   Hitchcock-DeGregori, S.E., Heald, R.W., 1987. Altered actin and troponin binding of amino-
1036   terminal variants of chicken striated muscle alpha-tropomyosin expressed in Escherichia
1037   coli. J. Biol. Chem. 262, 9730–5.

1038   Ho, J., Tumkaya, T., Aryal, S., Choi, H., Claridge-Chang, A., 2019. Moving beyond P values:
1039   data analysis with estimation graphics. Nat. Methods 16, 565–566.
1040   https://doi.org/10.1038/s41592-019-0470-3

1041   Holmes, K.C., Lehman, W., 2008. Gestalt-binding of tropomyosin to actin filaments. J. Muscle
1042   Res. Cell Motil. 29, 213–219. https://doi.org/10.1007/s10974-008-9157-6

1043   Hundt, N., Steffen, W., Pathan-Chhatbar, S., Taft, M.H., Manstein, D.J., 2016. Load-dependent
1044   modulation of non-muscle myosin-2A function by tropomyosin 4.2. Sci. Rep. 6, 20554.
1045   https://doi.org/10.1038/srep20554

1046   Ihnatovych, I., Migocka-Patrzalek, M., Dukh, M., Hofmann, W.A., 2012. Identification and
1047   characterization of a novel myosin Ic isoform that localizes to the nucleus. Cytoskeleton
1048   69, 555–565. https://doi.org/10.1002/cm.21040

1049   Janco, M., Bonello, T.T., Byun, A., Coster, A.C.F., Lebhar, H., Dedova, I., Gunning, P.W.,
1050   Böcking, T., 2016. The impact of tropomyosins on actin filament assembly is isoform
1051   specific. Bioarchitecture 6, 61–75. https://doi.org/10.1080/19490992.2016.1201619

1052   Johnson, C.A., Brooker, H.R., Gyamfi, I., O'Brien, J., Ashley, B., Brazier, J.E., Dean, A.,
1053   Embling, J., Grimsey, E., Tomlinson, A.C., Wilson, E.G., Geeves, M.A., Mulvihill, D.P.,
1054   2018. Temperature sensitive point mutations in fission yeast tropomyosin have long range
1055   effects on the stability and function of the actin-tropomyosin copolymer. Biochem.
1056   Biophys. Res. Commun. 506, 339–346. https://doi.org/10.1016/j.bbrc.2017.10.109

1057   Kabbage, M., Trimeche, M., ben Nasr, H., Hammann, P., Kuhn, L., Hamrita, B., Chahed, K.,
1058   2013. Tropomyosin-4 correlates with higher SBR grades and tubular differentiation in
1059   infiltrating ductal breast carcinomas: an immunohistochemical and proteomics-based
1060   study. Tumor Biol. 34, 3593–3602. https://doi.org/10.1007/s13277-013-0939-0

1061   Kee, A.J., Yang, L., Lucas, C.A., Greenberg, M.J., Martel, N., Leong, G.M., Hughes, W.E.,
1062   Cooney, G.J., James, D.E., Ostap, E.M., Han, W., Gunning, P.W., Hardeman, E.C., 2015.
1063   An Actin Filament Population Defined by the Tropomyosin Tpm3.1 Regulates Glucose
1064   Uptake. Traffic 16, 691–711. https://doi.org/10.1111/tra.12282

1065   Kovács, M., Wang, F., Hu, A., Zhang, Y., Sellers, J.R., 2003. Functional divergence of human
1066   cytoplasmic myosin II: kinetic characterization of the non-muscle IIA isoform. J. Biol.
1067   Chem. 278, 38132–40. https://doi.org/10.1074/jbc.M305453200

1068   Kron, S.J., Spudich, J.A., 1986. Fluorescent actin filaments move on myosin fixed to a glass
1069   surface. Proc. Natl. Acad. Sci. 83, 6272–6276. https://doi.org/10.1073/pnas.83.17.6272

1070   Latham, S.L., Ehmke, N., Reinke, P.Y.A., Taft, M.H., Eicke, D., Reindl, T., Stenzel, W.,
1071   Lyons, M.J., Friez, M.J., Lee, J.A., Hecker, R., Frühwald, M.C., Becker, K., Neuhann,
1072   T.M., Horn, D., Schrock, E., Niehaus, I., Sarnow, K., Grützmann, K., Gawehn, L., Klink,

B., Rump, A., Chaponnier, C., Figueiredo, C., Knöfler, R., Manstein, D.J., Di Donato, N., 2018. Variants in exons 5 and 6 of ACTB cause syndromic thrombocytopenia. Nat. Commun. 9, 4250. https://doi.org/10.1038/s41467-018-06713-0

Lehman, W., Moore, J.R., Campbell, S.G., Rynkiewicz, M.J., 2019. The Effect of Tropomyosin Mutations on Actin-Tropomyosin Binding: In Search of Lost Time. Biophys. J. 116, 2275–2284. https://doi.org/10.1016/j.bpj.2019.05.009

Lehrer, S.S., Kerwar, G., 1972. Intrinsic fluorescence of actin. Biochemistry 11, 1211–7. https://doi.org/10.1021/bi00757a015

Levitsky, D.I., Rostkova, E. V., Orlov, V.N., Nikolaeva, O.P., Moiseeva, L.N., Teplova, M. V., Gusev, N.B., 2000. Complexes of smooth muscle tropomyosin with F-actin studied by differential scanning calorimetry. Eur. J. Biochem. 267, 1869–1877. https://doi.org/10.1046/j.1432-1327.2000.01192.x

Li, X.E., Holmes, K.C., Lehman, W., Jung, H., Fischer, S., 2010. The shape and flexibility of tropomyosin coiled coils: implications for actin filament assembly and regulation. J. Mol. Biol. 395, 327–39. https://doi.org/10.1016/j.jmb.2009.10.060

Lin, J.J.C., Warren, K.S., Wamboldt, D.D., Wang, T., Lin, J.L.C., 1997. Tropomyosin isoforms in nonmuscle cells. Int. Rev. Cytol. 170, 1–39. https://doi.org/10.1016/s0074-7696(08)61619-8

Manstein, D.J., Mulvihill, D.P., 2016. Tropomyosin-Mediated Regulation of Cytoplasmic Myosins. Traffic 17, 872–877. https://doi.org/10.1111/tra.12399

Marchenko, M., Nefedova, V., Artemova, N., Kleymenov, S., Levitsky, D., Matyushenko, A., 2021. Structural and Functional Peculiarities of Cytoplasmic Tropomyosin Isoforms, the Products of TPM1 and TPM4 Genes. Int. J. Mol. Sci. 22, 5141. https://doi.org/10.3390/ijms22105141

Marston, S.B., Copeland, O., Messer, A.E., MacNamara, E., Nowak, K., Zampronio, C.G., Ward, D.G., 2013. Tropomyosin isoform expression and phosphorylation in the human heart in health and disease. J. Muscle Res. Cell Motil. 34, 189–197. https://doi.org/10.1007/s10974-013-9347-8

Maytum, R., Geeves, M.A., Konrad, M., 2000. Actomyosin Regulatory Properties of Yeast Tropomyosin Are Dependent upon N-Terminal Modification[†]. Biochemistry 39, 11913–11920. https://doi.org/10.1021/bi000977g

Maytum, R., Konrad, M., Lehrer, S.S., Geeves, M.A., 2001. Regulatory properties of tropomyosin effects of length, isoform, and N-terminal sequence. Biochemistry 40, 7334–41. https://doi.org/10.1021/bi010072i

McIntosh, B.B., Holzbaur, E.L.F., Ostap, E.M., 2015. Control of the initiation and termination of kinesin-1-driven transport by myosin-Ic and nonmuscle tropomyosin. Curr. Biol. 25, 523–9. https://doi.org/10.1016/j.cub.2014.12.008

McLachlan, A.D., Stewart, M., 1976. The 14-fold periodicity in alpha-tropomyosin and the interaction with actin. J. Mol. Biol. 103, 271–98.

Mehta, A.D., Rock, R.S., Rief, M., Spudich, J.A., Mooseker, M.S., Cheney, R.E., 1999. Myosin-V is a processive actin-based motor. Nature 400, 590–593. https://doi.org/10.1038/23072

Meiring, J.C.M., Bryce, N.S., Lastra Cagigas, M., Benda, A., Whan, R.M., Ariotti, N., Parton, R.G., Stear, J.H., Hardeman, E.C., Gunning, P.W., 2019. Colocation of Tpm3.1 and myosin IIa heads defines a discrete subdomain in stress fibres. J. Cell Sci. 132.

36

1118   https://doi.org/10.1242/jcs.228916

1119 Meiring, J.C.M., Bryce, N.S., Wang, Y., Taft, M.H., Manstein, D.J., Liu Lau, S., Stear, J.,
1120   Hardeman, E.C., Gunning, P.W., 2018. Co-polymers of Actin and Tropomyosin Account
1121   for a Major Fraction of the Human Actin Cytoskeleton. Curr. Biol. 28, 2331-2337.e5.
1122   https://doi.org/10.1016/j.cub.2018.05.053

1123 Monteiro, P.B., Lataro, R.C., Ferro, J.A., Reinach, F. de C., 1994. Functional alpha-
1124   tropomyosin produced in Escherichia coli. A dipeptide extension can substitute the amino-
1125   terminal acetyl group. J. Biol. Chem. 269, 10461–6.

1126 Moraczewska, J., Nicholson-Flynn, K., Hitchcock-Degregori, S.E., 1999. The ends of
1127   tropomyosin are major determinants of actin affinity and myosin subfragment 1-induced
1128   binding to F-actin in the open state. Biochemistry 38, 15885–15892.
1129   https://doi.org/10.1021/bi991816j

1130 Müller, M., Diensthuber, R.P., Chizhov, I., Claus, P., Heissler, S.M., Preller, M., Taft, M.H.,
1131   Manstein, D.J., 2013. Distinct functional interactions between actin isoforms and
1132   nonsarcomeric myosins. PLoS One 8, e70636.
1133   https://doi.org/10.1371/journal.pone.0070636

1134 Münnich, S., Manstein, D.J., 2013. Expression, purification, crystallization and preliminary X-
1135   ray crystallographic analysis of human myosin 1c in complex with calmodulin. Acta
1136   Crystallogr. Sect. F. Struct. Biol. Cryst. Commun. 69, 1020–2.
1137   https://doi.org/10.1107/S1744309113020988

1138 Münnich, S., Taft, M.H., Manstein, D.J., 2014. Crystal structure of human myosin 1c--the
1139   motor in GLUT4 exocytosis: implications for Ca2+ regulation and 14-3-3 binding. J. Mol.
1140   Biol. 426, 2070–81. https://doi.org/10.1016/j.jmb.2014.03.004

1141 Ngo, K.X., Umeki, N., Kijima, S.T., Kodera, N., Ueno, H., Furutani-Umezu, N., Nakajima, J.,
1142   Noguchi, T.Q.P., Nagasaki, A., Tokuraku, K., Uyeda, T.Q.P., 2016. Allosteric regulation
1143   by cooperative conformational changes of actin filaments drives mutually exclusive
1144   binding with cofilin and myosin. Sci. Rep. 6, 35449. https://doi.org/10.1038/srep35449

1145 Noguchi, T.Q.P., Kanzaki, N., Ueno, H., Hirose, K., Uyeda, T.Q.P., 2007. A novel system for
1146   expressing toxic actin mutants in Dictyostelium and purification and characterization of a
1147   dominant lethal yeast actin mutant. J. Biol. Chem. 282, 27721–7.
1148   https://doi.org/10.1074/jbc.M703165200

1149 Nowak, G., Pestic-Dragovich, L., Hozák, P., Philimonenko, A., Simerly, C., Schatten, G., de
1150   Lanerolle, P., 1997. Evidence for the presence of myosin I in the nucleus. J. Biol. Chem.
1151   272, 17176–81. https://doi.org/10.1074/jbc.272.27.17176

1152 Orzechowski, M., Li, X.E., Fischer, S., Lehman, W., 2014. An atomic model of the
1153   tropomyosin cable on F-actin. Biophys. J. 107, 694–699.
1154   https://doi.org/10.1016/j.bpj.2014.06.034

1155 Palm, T., Greenfield, N.J., Hitchcock-DeGregori, S.E., 2003. Tropomyosin Ends Determine
1156   the Stability and Functionality of Overlap and Troponin T Complexes. Biophys. J. 84,
1157   3181. https://doi.org/10.1016/S0006-3495(03)70042-3

1158 Parry, D.A.D., Squire, J.M., 1973. Structural role of tropomyosin in muscle regulation:
1159   Analysis of the X-ray diffraction patterns from relaxed and contracting muscles. J. Mol.
1160   Biol. 75, 33–55. https://doi.org/10.1016/0022-2836(73)90527-5

1161 Pathan-Chhatbar, S., Taft, M.H., Reindl, T., Hundt, N., Latham, S.L., Manstein, D.J., 2018.
1162   Three mammalian tropomyosin isoforms have different regulatory effects on nonmuscle

myosin-2B and filamentous β-actin *in vitro*. J. Biol. Chem. 293, 863–875. https://doi.org/10.1074/jbc.M117.806521

Pelham, R.J., Lin, J.J., Wang, Y.L., 1996. A high molecular mass non-muscle tropomyosin isoform stimulates retrograde organelle transport. J. Cell Sci. 109, 981 LP – 989.

Pertici, I., Bongini, L., Melli, L., Bianchi, G., Salvi, L., Falorsi, G., Squarci, C., Bozó, T., Cojoc, D., Kellermayer, M.S.Z., Lombardi, V., Bianco, P., 2018. A myosin II nanomachine mimicking the striated muscle. Nat. Commun. 9, 3532. https://doi.org/10.1038/s41467-018-06073-9

Pittenger, M.F., Kazzaz, J.A., Helfman, D.M., 1994. Functional properties of non-muscle tropomyosin isoforms. Curr. Opin. Cell Biol. 6, 96–104. https://doi.org/10.1016/0955-0674(94)90122-8

Pleines, I., Woods, J., Chappaz, S., Kew, V., Foad, N., Ballester-Beltrán, J., Aurbach, K., Lincetto, C., Lane, R.M., Schevzov, G., Alexander, W.S., Hilton, D.J., Astle, W.J., Downes, K., Nurden, P., Westbury, S.K., Mumford, A.D., Obaji, S.G., Collins, P.W., Delerue, F., Ittner, L.M., Bryce, N.S., Holliday, M., Lucas, C.A., Hardeman, E.C., Ouwehand, W.H., Gunning, P.W., Turro, E., Tijssen, M.R., Kile, B.T., Kile, B.T., 2017. Mutations in tropomyosin 4 underlie a rare form of human macrothrombocytopenia. J. Clin. Invest. 127, 814–829. https://doi.org/10.1172/JCI86154

Preller, M., Manstein, D.J., 2013. Myosin structure, allostery, and mechano-chemistry. Structure 21, 1911–22. https://doi.org/10.1016/j.str.2013.09.015

Redwood, C., Robinson, P., 2013. Alpha-tropomyosin mutations in inherited cardiomyopathies. J. Muscle Res. Cell Motil. 34, 285–294. https://doi.org/10.1007/s10974-013-9358-5

Reumiller, C.M., Schmidt, G.J., Dhrami, I., Umlauf, E., Rappold, E., Zellner, M., 2018. Gender-related increase of tropomyosin-1 abundance in platelets of Alzheimer's disease and mild cognitive impairment patients. J. Proteomics 178, 73–81. https://doi.org/10.1016/j.jprot.2017.12.018

Rock, R.S., Rief, M., Mehta, A.D., Spudich, J.A., 2000. In Vitro Assays of Processive Myosin Motors. Methods 22, 373–381. https://doi.org/10.1006/METH.2000.1089

Sao, K., Jones, T.M., Doyle, A.D., Maity, D., Schevzov, G., Chen, Y., Gunning, P.W., Petrie, R.J., 2019. Myosin II governs intracellular pressure and traction by distinct tropomyosin-dependent mechanisms. Mol. Biol. Cell 30, 1170–1181. https://doi.org/10.1091/mbc.E18-06-0355

Schevzov, G., Whittaker, S.P., Fath, T., Lin, J.J., Gunning, P.W., 2011. Tropomyosin isoforms and reagents. Bioarchitecture 1, 135–164. https://doi.org/10.4161/bioa.1.4.17897

Schindelin, J., Arganda-Carreras, I., Frise, E., Kaynig, V., Longair, M., Pietzsch, T., Preibisch, S., Rueden, C., Saalfeld, S., Schmid, B., Tinevez, J.-Y., White, D.J., Hartenstein, V., Eliceiri, K., Tomancak, P., Cardona, A., 2012. Fiji: an open-source platform for biological-image analysis. Nat. Methods 9, 676–682. https://doi.org/10.1038/nmeth.2019

Schmidt, W.M., Lehman, W., Moore, J.R., 2015. Direct observation of tropomyosin binding to actin filaments. Cytoskeleton (Hoboken). 72, 292–303. https://doi.org/10.1002/cm.21225

Sckolnick, M., Krementsova, E.B., Warshaw, D.M., Trybus, K.M., 2016. Tropomyosin isoforms bias actin track selection by vertebrate myosin Va. Mol. Biol. Cell 27, 2889. https://doi.org/10.1091/MBC.E15-09-0641

1208 Silva, R.D., Martinho, R.G., 2015. Developmental roles of protein N-terminal acetylation.
1209   Proteomics 15, 2402–2409. https://doi.org/10.1002/pmic.201400631

1210 Spudich, J.A., Huxley, H.E., Finch, J.T., 1972. Regulation of skeletal muscle contraction. II.
1211   Structural studies of the interaction of the tropomyosin-troponin complex with actin. J.
1212   Mol. Biol. 72, 619–32.

1213 Spudich, J.A., Watt, S., 1971. The regulation of rabbit skeletal muscle contraction. I.
1214   Biochemical studies of the interaction of the tropomyosin-troponin complex with actin
1215   and the proteolytic fragments of myosin. J. Biol. Chem. 246, 4866–71.

1216 Stefen, H., Suchowerska, A.K., Chen, B.J., Brettle, M., Kuschelewski, J., Gunning, P.W.,
1217   Janitz, M., Fath, T., 2018. Tropomyosin isoforms have specific effects on the
1218   transcriptome of undifferentiated and differentiated B35 neuroblastoma cells. FEBS Open
1219   Bio 8, 570–583. https://doi.org/10.1002/2211-5463.12386

1220 Stehn, J.R., Haass, N.K., Bonello, T., Desouza, M., Kottyan, G., Treutlein, H., Zeng, J.,
1221   Nascimento, P.R.B.B., Sequeira, V.B., Butler, T.L., Allanson, M., Fath, T., Hill, T.A.,
1222   McCluskey, A., Schevzov, G., Palmer, S.J., Hardeman, E.C., Winlaw, D., Reeve, V.E.,
1223   Dixon, I., Weninger, W., Cripe, T.P., Gunning, P.W., 2013. A novel class of anticancer
1224   compounds targets the actin cytoskeleton in tumor cells. Cancer Res. 73, 5169–82.
1225   https://doi.org/10.1158/0008-5472.CAN-12-4501

1226 Stehn, J.R., Schevzov, G., O'Neill, G.M., Gunning, P.W., 2006. Specialisation of the
1227   tropomyosin composition of actin filaments provides new potential targets for
1228   chemotherapy. Curr. Cancer Drug Targets 6, 245–56.

1229 Tobacman, L.S., 2008. Cooperative binding of tropomyosin to actin. Adv. Exp. Med. Biol.
1230   644, 85–94. https://doi.org/10.1007/978-0-387-85766-4_7

1231 Toyoshima, Y.Y., Toyoshima, C., Spudich, J.A., 1989. Bidirectional movement of actin
1232   filaments along tracks of myosin heads. Nature 341, 154–6.
1233   https://doi.org/10.1038/341154a0

1234 Urbancikova, M., Hitchcock-DeGregori, S.E., 1994. Requirement of amino-terminal
1235   modification for striated muscle alpha-tropomyosin function. J. Biol. Chem. 269, 24310–
1236   5.

1237 Uyeda, T.Q., Kron, S.J., Spudich, J.A., 1990. Myosin step size. Estimation from slow sliding
1238   movement of actin over low densities of heavy meromyosin. J. Mol. Biol. 214, 699–710.
1239   https://doi.org/10.1016/0022-2836(90)90287-V

1240 Vilfan, A., 2001. The Binding Dynamics of Tropomyosin on Actin. Biophys. J. 81, 3146–3155.
1241   https://doi.org/10.1016/S0006-3495(01)75951-6

1242 von der Ecken, J., Müller, M., Lehman, W., Manstein, D.J., Penczek, P.A., Raunser, S., 2015.
1243   Structure of the F-actin–tropomyosin complex. Nature 519, 114–117.
1244   https://doi.org/10.1038/nature14033

1245 Vrhovski, B., Schevzov, G., Dingle, S., Lessard, J.L., Gunning, P., Weinberger, R.P., 2003.
1246   Tropomyosin isoforms from the gamma gene differing at the C-terminus are spatially and
1247   developmentally regulated in the brain. J. Neurosci. Res. 72, 373–83.
1248   https://doi.org/10.1002/jnr.10586

1249 Wegner, A., 1980. The interaction of α,α- and α,β-tropomyosin with actin filaments. FEBS
1250   Lett. 119, 245–248. https://doi.org/10.1016/0014-5793(80)80263-8

1251 Wegner, A., 1979. Equilibrium of the actin-tropomyosin interaction. J. Mol. Biol. 131, 839–
1252   853. https://doi.org/10.1016/0022-2836(79)90204-3

1253   Weigt, C., Wegner, A., Koch, M.H., 1991. Rate and mechanism of the assembly of
1254   tropomyosin with actin filaments. Biochemistry 30, 10700–10707.

1255   Wolfenson, H., Meacci, G., Liu, S., Stachowiak, M.R., Iskratsch, T., Ghassemi, S., Roca-
1256   Cusachs, P., O'Shaughnessy, B., Hone, J., Sheetz, M.P., 2016. Tropomyosin controls
1257   sarcomere-like contractions for rigidity sensing and suppressing growth on soft matrices.
1258   Nat. Cell Biol. 18, 33–42. https://doi.org/10.1038/ncb3277

1259   Zattelman, L., Regev, R., Ušaj, M., Reinke, P.Y.A., Giese, S., Samson, A.O., Taft, M.H.,
1260   Manstein, D.J., Henn, A., 2017. N-terminal splicing extensions of the human MYO1C
1261   gene fine-tune the kinetics of the three full-length myosin IC isoforms. J. Biol. Chem.
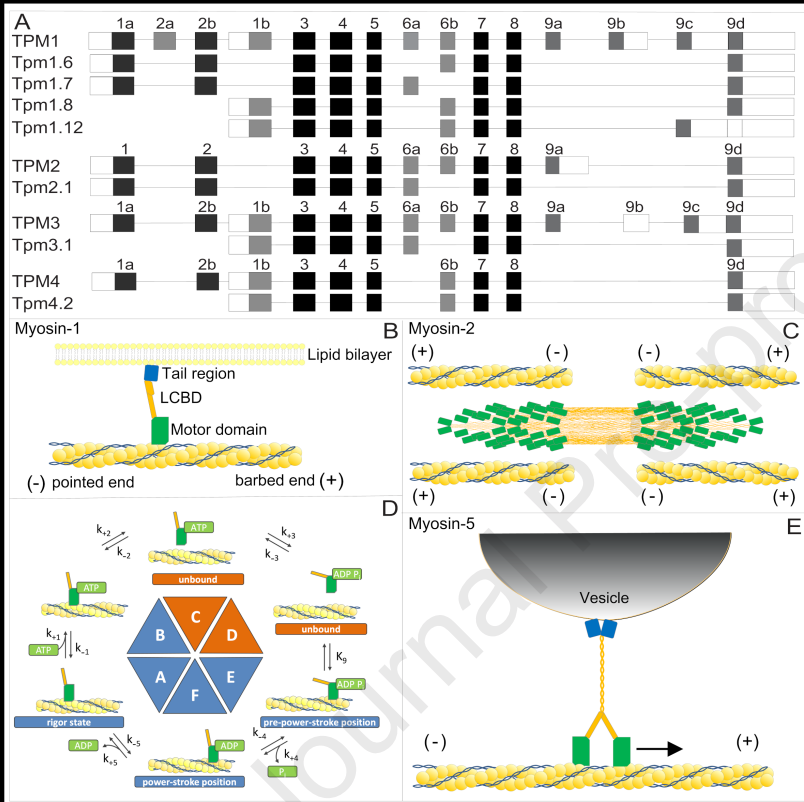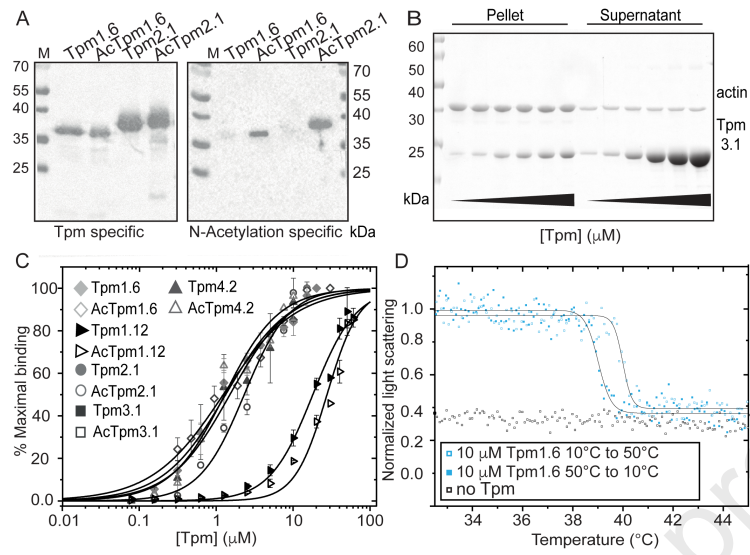1262   292, 17804–17818. https://doi.org/10.1074/jbc.M117.794008
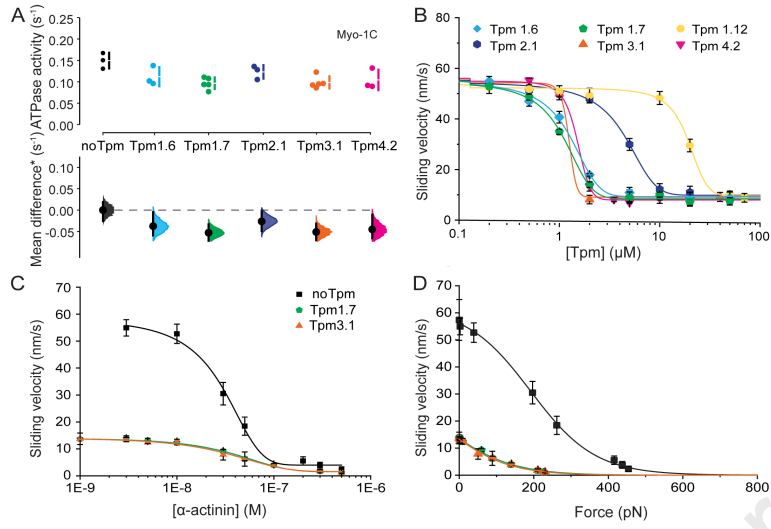
1263

1264

1265

1266

Figure 2

Figure 3
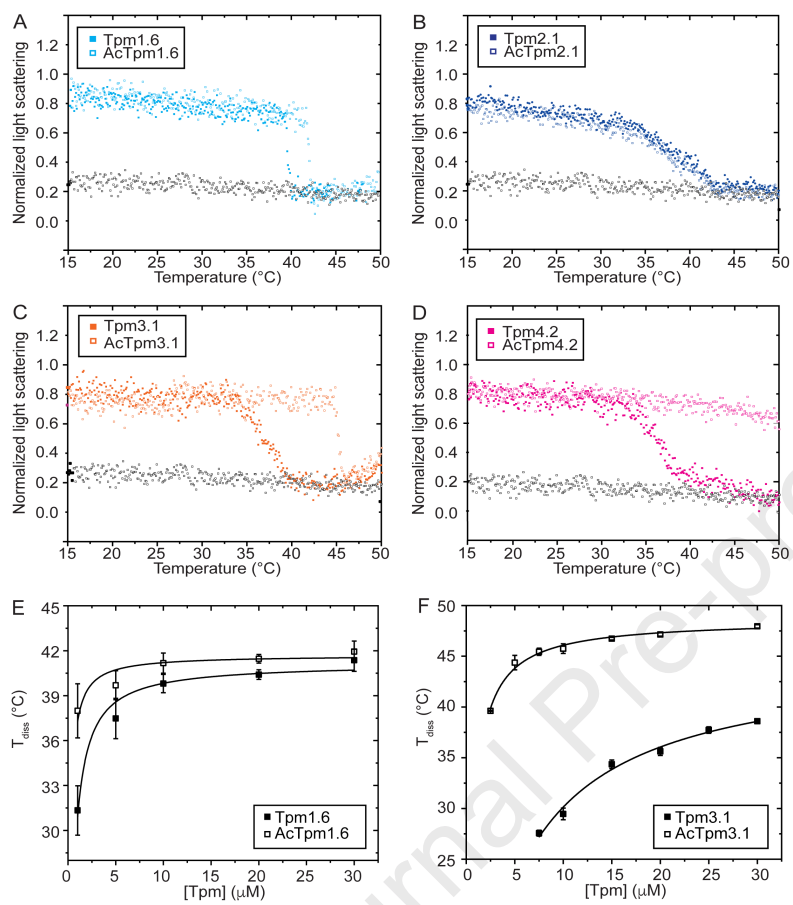
Figure 4

Figure 5

Figure 7

A

ATPase activity (s⁻¹)
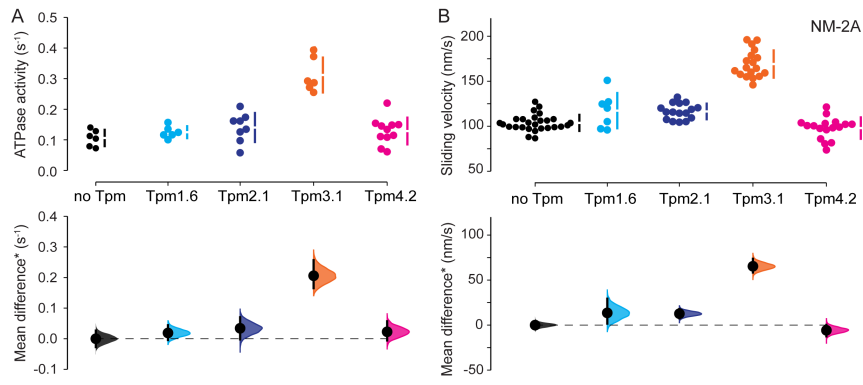
Myosin-5A

Mean difference* (s)

B

Sliding velocity (nm/s)

Mean difference* (nm/s)
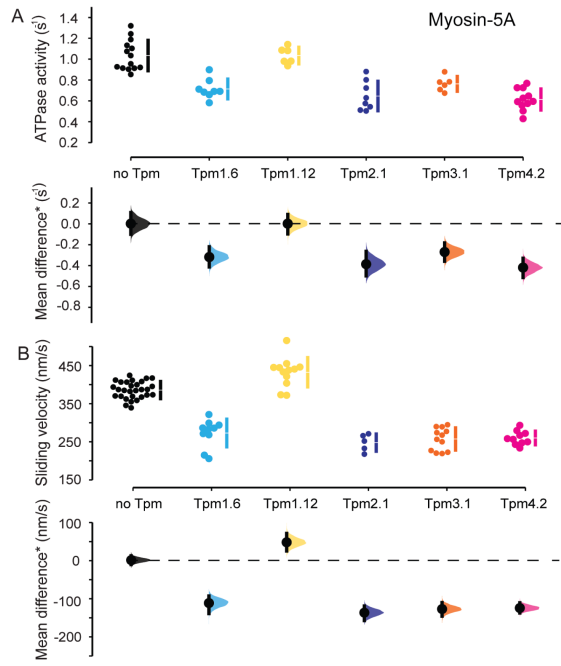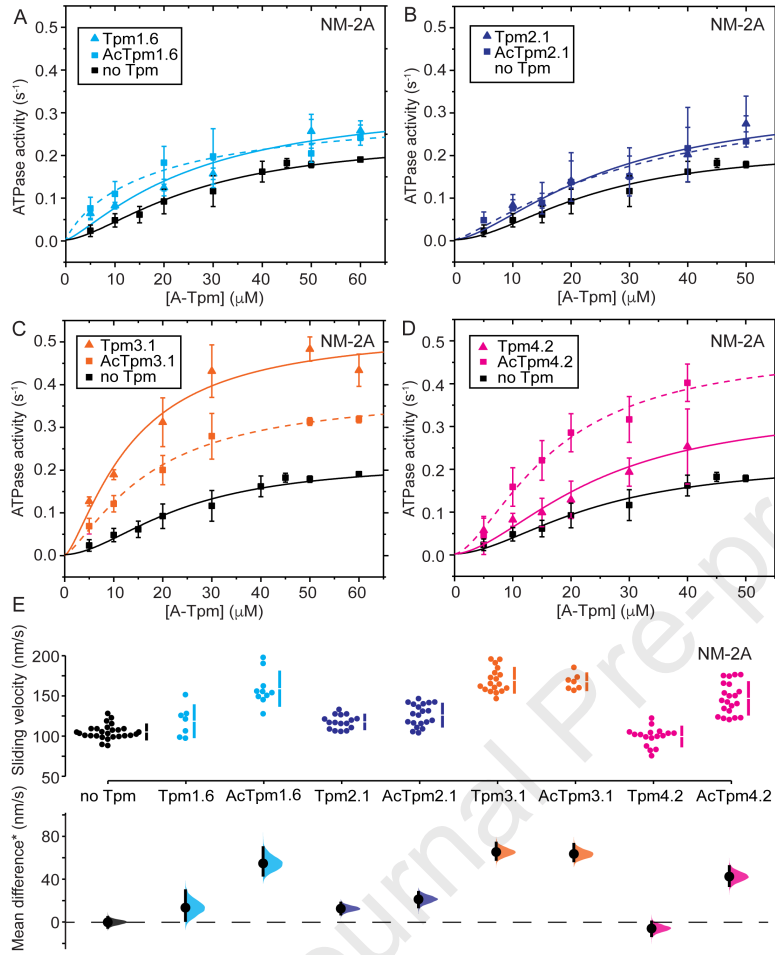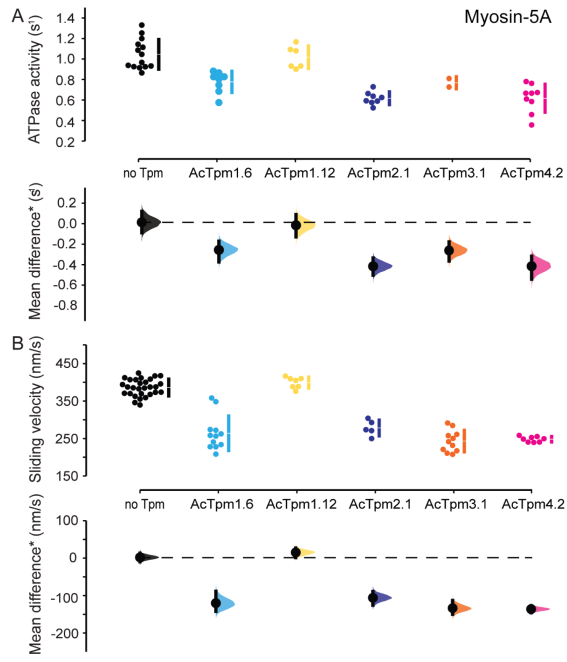
HIGHLIGHTS

- Tpm diversity is largely determined by sequences contributing to the overlap region

- Global sequence differences are of greater importance than variable exon 6 usage

- Tpm isoforms confer distinctly altered properties to cytoskeletal myosin motors

- Cytoskeletal myosins are differentially affected by N-terminal acetylation of Tpm

TABLE FOR AUTHOR TO COMPLETE

Please upload the completed table as a separate document. **Please do not add subheadings to the key resources table.** *If you wish to make an entry that does not fall into one of the subheadings below, please contact your handling editor.* **Any subheadings not relevant to your study can be skipped.** (**NOTE:** *For authors publishing in Cell Genomics, Cell Reports Medicine, Current Biology, and Med, please note that references within the KRT should be in numbered style rather than Harvard.*)

Key resources table

REAGENT or RESOURCE	SOURCE	IDENTIFIER
Antibodies		
Mouse monoclonal antibody QIAexpress Penta·His	Qiagen	Cat#34650
Sheep polyclonal antibody TPM3/9d	Merck Millipore	Cat#AB5447
Sheep polyclonal antibody TPM1/1b	Merck Millipore	Cat#ABC499
Sheep polyclonal antibody TPM1/9d	Merck Millipore	Cat#AB5441
Donkey anti–sheep IgG–HRP secondary antibody	Santa Cruz Biotechnology	Cat#sc–2473
Rabbit polyclonal antibody D55Ac	Eurogentec	N/A
Bacterial and virus strains		
E. coli Rosetta pLys-S	Merck Millipore	Cat#70956
E. coli BL21(DE3)	Thermo Fisher Scientific	Cat#EC0114
E. coli DH10Bac	Thermo Fisher Scientific	Cat#10361012
Chemicals, peptides, and recombinant proteins		
Phalloidin–tetramethyl rhodamine B isothiocyanate	Merck Millipore	Cat#P1951
Myosin light chain kinase	abcam	Cat#ab55674
Lactate dehydrogenase from rabbit muscle	Roche Diagnostics	Cat#10127876001
Pyruvate kinase from rabbit muscle	Roche Diagnostics	Cat#10128155001
Catalase from bovine liver	Merck Millipore	Cat#C9322
Glucose oxidase from *aspergillus niger*	Merck Millipore	Cat#G7141
Experimental models: Cell lines		
*Sf*9 cells adapted to Sf-900™ II SFM	Thermo Fisher Scientific	Cat#11496015
Oligonucleotides		
See Table S1 for oligonucleotide sequences		
Recombinant DNA		
Plasmid: pET–3a	Merck Millipore	Cat#69418
Plasmid: pET–3d	Merck Millipore	Cat#69421
Plasmid: pET–23a(+)	Merck Millipore	Cat#69771
Plasmid: pRHA-67	Daniel P. Mulvihill, University of Kent, Canterbury, UK	N/A
Plasmid: pFastBac 1	Thermo Fisher Scientific	Cat#10360014
Plasmid: pFastBac Dual	Thermo Fisher Scientific	Cat#10712024
Human Myo1C^0–ΔTH1 cDNA	Giese et al., 2020	NM_001080779.1; aa residues 1–856

Human NM–2A cDNA	Hundt et al., 2016	NM_002473.5 ; aa residues 1–1337
Human Myosin–5A cDNA	This paper	NM_000259.3; aa residues 1–1098
Human Calmodulin–1 cDNA	This paper	NM_001329922.1
Human non–muscle essential light chain (MYL6) cDNA	Hundt et al., 2016	NM_021019.4
Human non–muscle regulatory light chain (MYL12b) cDNA	Hundt et al., 2016	NM_001144944.1
Human β–actin cDNA	Müller et al., 2013	NM_001101.3
Human γ–actin cDNA	Müller et al., 2013	NM_001199954.1
Human Tpm1.6 cDNA	This paper	NM_001018004.2
Human Tpm1.7 cDNA	This paper	NM_001018006.2
Human Tpm1.8 cDNA	Pathan-Chhatbar et al., 2018	NM_001301289.2
Human Tpm1.12 cDNA	Pathan-Chhatbar et al., 2018	NM_001018008.2
Human Tpm2.1 cDNA	This paper	NM_213674.1
Human Tpm3.1 cDNA	Pathan-Chhatbar et al., 2018	NM_153649.4
Human Tpm4.2 cDNA	Hundt et al., 2016	NM_003290.3
Fission yeast Naa10 cDNA	Eastwood et al., 2017	NM_001019732.2
Fission yeast Naa15 cDNA	Eastwood et al., 2017	NM_001023149.2
Fission yeast Naa20 cDNA	Eastwood et al., 2017	NM_001022913.2
Fission yeast Naa25 cDNA	Eastwood et al., 2017	NM_001021526.2
Software and algorithms		
ImageJ	Schindelin et al., 2012	https://imagej.nih.gov/ij/
ImageJ plugin *wrMTrck*	Jesper Søndergaard Pedersen (jsp@phage.dk)	https://www.phage.dk/plugins/wrmtrck.html
Python	-	https://www.python.org/downloads/
DABEST plugin for Python	Ho, Tumkaya, Aryal, Choi, & Claridge-Chang, 2019	https://github.com/ACCLAB/DABEST-python
Kinetic Studio 4.07	TgK Scientific Limited, Bradford on Avon, UK	https://www.hi-techsci.com/instruments/kinetic-studio/
Origin Pro 9.55	Originlab, Massachusetts, USA	https://www.originlab.com/